Biomolecular photosensitizers for dye-sensitized solar cells: Recent developments and critical insights

Hisham A. Maddah [a,b], Vikas Berry [a], Sanjay K. Behura [a,*]

[a] Department of Chemical Engineering, University of Illinois at Chicago, 945 W. Taylor St., Engineering Innovation Building, Chicago, IL, 60607, United States
[b] Department of Chemical Engineering, King Abdulaziz University, Rabigh 21911, Saudi Arabia

ARTICLE INFO

ABSTRACT

Dye-sensitized solar cells based on bacterial-based photosensitizers (bio-sensitized DSSCs) are promising bio-photoelectronic molecular devices exhibiting enhanced electron excitation, injection, and dye regeneration for efficient photon-to-electron quantum-conversion. Achieving high DSSCs performance *via* environmentally sustainable, cost-effective, and naturally-sensitized plant-based or bacterial-based biomolecules remains a challenge. Here, we provide a comprehensive study on the mechanisms involved in the utilization of biomolecular bacterial-based pigments (e.g. proteins and carotenoids) for an improved bio-sensitized DSSCs performance. Protein complexes and chlorophyll a/carotenoids are among many bio-photosensitizers demonstrating high incident photon-to-current efficiency (IPCE). Pigments molecular structure, donor-π-acceptor conjugation, and anchoring groups have been discussed and attributed to theoretical dye HOMO–LUMO bandgaps and their corresponding bio-sensitized DSSCs IPCE. This review provides critical understanding of advancements towards natural photosensitization: (i) carboxyl/hydroxyl groups attached to acceptor segments provide firm attachment and rapid electron injection, (ii) proteins/carotenoids hybrid dyes induce visible-light photosensitivity and broaden absorbance, (iii) increased conjugated π-bonds (n > 13) develop pigment visible-NIR absorption with intensified photoactivity, (iv) chromatophores integrated with bio-electrolyte provide a unidirectional flow of electrons, (v) reaction center (RC)-sensitized DSSCs have better optoelectronic properties than light-harvesting complex (LH2) due to its efficient charge separation, (vi) antioxidants hinder degradation of pigmented-photoanodes from UV radiation, (vii) solid-state redox improves device stability and dye neutralization; which all together would boost the dye sensitization performance in bio-sensitized DSSCs. The highest recorded IPCEs are found for TiO_2-based DSSCs using plant-based coumarin (9%) and from [A. amentacea + P. pterocarpum] pigments (8.22%). Futuristically, we anticipate that these biologically-derived photosensitizers can be integrated into photoanodes for photoelectronic applications including DSSCs, multi-junction cells, photodiodes, photo-transistors, photodetectors, flexible bioelectronic films and clothes, bio-LEDs, and photo-tunneling junctions.

1. Introduction

Non-renewable energy resources such as fossil fuels pose environmental concerns and will be diminished due to the limited oil/gas reserves as well as the increasing demand for energy. Econometric models estimated that fossil fuel reserves will be totally consumed by the year 2042 [1]. In contrast, solar energy is the most abundant, unlimited, free, and environmental-friendly energy with power approximately 1.8×10^{11} MW from sun intercepted by the earth [2]. Photovoltaics (PV) is an efficient tool designed to harness the solar power by converting incident photons to excitons for electricity generation [2]. However, commercial silicon-based solar cells (first-generation) are expensive to manufacture and are restricted to the terrestrial PV market only as compared to the second-generation PV systems (multi-crystalline Si) [3–7] and the emerging third-generation PV systems such as organic/inorganic perovskite solar cells [8–16], inorganic solar cells (Si, III-V compounds, alloys, CdTe, CIGS) [17–24], organic tandem solar cells [25–31], quantum dot solar cells [32–37], and dye-sensitized solar cells (DSSCs) [38–48], which are still in the development phase for being commercialized [49]. In 1991, O'Regan and Grätzel [38] initiated the idea of DSSCs inspired by natural photosynthesis and photography processes [50]. Similar to natural photosynthesis, DSSCs utilize plants and fruits pigment molecules to transfer energy and electrons converting light

---

Nomenclature (i.e. abbreviations, notation and units)

DSSCs	Dye-sensitized solar cells
PV	Photovoltaics
LH	Light harvesting
RC	Reaction center
BChl	Bacteriochlorophyll a (PPB a)
PPCs	Proteins pigment complexes (LH2, BR, RC)
LHCII	Light-harvesting complex II
PSI	Photosystem I trimer
TCO	Transparent conductive oxide
ITO	Indium tin oxide
FTO	Fluorine doped tin oxide
S	Ground state
S*	Higher or excited energy state
S$^+$	Oxidized-dye
I^-/I_3^-	Redox mediator
I_3^-	Iodide
$3I^-$	Triiodide
SWCNTs	Single-walled carbon nanotubes
N-GNRs	Nitrogen-doped graphene nanoribbons
3DG	Three-dimensional graphene-based
3DGNs	Three-dimensional graphene networks
rGO	Reduced graphene oxide
UV	Ultraviolet
CEs	Counter electrodes
BR	Bacteriorhodopsin (protein) or Bacterioruberin (carotenoid)
Spx	Spirilloxanthin
CSSC	Chromatophores sensitized solar cell
Q0	Quinone
AM1.5	Air mass (100 mW cm^{-2})
DFT	Density functional theory
DPP	Diketopyrrolopyrrole
C_8H_9N	Indolines
C-QDs	Carbon quantum dots
TD-DFT	Time dependent and density functional theory
Bio-LEDs	Bio-light-emitting diodes
I_{cell}/mA	Total cell current
KVL/V	Kirchhoffs's voltage
I_{ph}/mA	Cell photo-generated current
I_0/mA	Dark saturation current
I_r/mA	Back reaction (recombination) current
I_{sh}/mA	Shunt (leakage) current
V_{PE}/V	Photoanode electrode voltage
I_{sh}/mA	Shunt current
R_s/Ω	Series resistance
R_{sh}/Ω	Shunt resistance
R_r/Ω	Recombination resistance
V_{cell}/V	Applied cell voltage
I_r/mA	Recombination current
q	Electron charge (1.602×10^{-18} C)
n	Ideality factor
k_B	Boltzmann constant (1.38×10^{-23} J K^{-1})
T/K	Absolute temperature
V_{oc}/V	Open-circuit voltage
I_{sc}/mA	Short-circuit current (or J$_{sc}$ as current density in mA cm^{-2})
FF	Fill factor
PCE/%	Power conversion efficiency
E$_F$/eV	Fermi level
E$_{CB}$/eV	Conduction band edge
E$_a$/eV	Activation energy
HOMO	Highest occupied molecular orbital (ground state)
LUMO	Lowest unoccupied molecular orbital (excited state)
IPCE/%	Incident photon-to-current efficiency
QE/%	Quantum efficiency
E$_g$/eV	Bandgap energies arise from the difference between HOMO to LUMO levels
EMIM-I	2-methylImmidazolium iodide
BDH	Sodium iodide
PEO	poly(ethylene)oxide
C_8H_7N	Indoles
G-QDs	Graphene quantum-dots
SFX	Spiro[fluorene-9,9′-xanthene] hole transporting materials (HTM)
CB	Conduction band

---

energy into electricity (instead of the chemical energy conversion stored as sugars and carbohydrates in natural photosynthesis). Thus, DSSC (Grätzel cell) is defined as a thin-film photovoltaic (solar) cell that efficiently converts any visible-light into electrical energy.

An intense research work [38] has been devoted to DSSCs from 1991 to 2014 which resulted in improving DSSCs efficiency from 7.1% to 13% for commercialization viability [51]. In 2015, Ye et al. reported a maximum DSSC efficiency of 15% achieved with a solid-state mesoscopic TiO$_2$ DSSC sensitized with lead iodide perovskite (CH$_3$NH$_3$PbI$_3$) under AM1.5 illumination; which is expected to reach a ~20% future cell performance. The maximum recorded efficiency of commercial crystalline silicon solar cells is approximately 25% ($2.7–3.57/W) [52]. However, DSSCs are cost-effective solar cells (<$0.5/W) owing to their inexpensive materials/components and explicit fabrication design with little maintenance requirements [2,40,49]. A typical DSSC system includes four major components: photoanode, photosensitizer, electrolyte, and counter electrode (cathode) [49]. The cell converts visible-light energy into electrical energy by sensitizing a wide bandgap semiconductor (e.g. TiO$_2$, ZnO, and SnO$_2$) to inject a photo-excited electron at the interface between the semiconductor material and the monolayer sensitizer [50]. Nanoporous large-area semiconductors provide anchoring sites for dye molecules acceptor segments for easy electron injection from the generated electron-hole (e-h) pairs. Charge separation

occurs in femtoseconds due to the electron injection from the dye molecules into the conduction band (CB) of the semiconductor [41,53]. To date, commercial photosensitizers used in DSSCs are limited to plant-based organic dyes [43], ruthenium dyes [54], and platinum dyes [55]. However, inorganic dyes are scarce in nature, synthetically produced, very expensive, and pose a high risk of toxicity to humans (ecosystem pollution) [56]. Thus, research efforts have been shifted to focus on natural photosensitizers, and specifically on biomolecular sensitizers from bacterial sources such as naturally optimized light harvesting (LH) ligands, photochemical reaction center (RC) protein, and carotenoid complexes for photons-to-electrons conversion [57].

The chemical structure of a photosensitizer material involves a donor-acceptor-substituted π-conjugated bridge (D–π–A), Fig. 1(A).The dye's anchoring group exists in the acceptor part allows dye molecules to chemically attach themselves to the semiconductor surface [58]. Anchoring groups in dye molecules bind to oxide layers *via* a surface hydroxylation chemical reaction [59]. Covalently-bonded dye particles reduce interfacial resistance for the electron flow. Perfect bonding and dye attachment occur from surface interaction between functional groups as carboxyl and/or other peripheral acidic anchoring groups with the semiconductor surface. Earlier works [60] suggest that acidic dye solutions are preferred since de-attachment of dye molecules usually occur around pH = 9. A photosensitizer is considered efficient for DSSCs
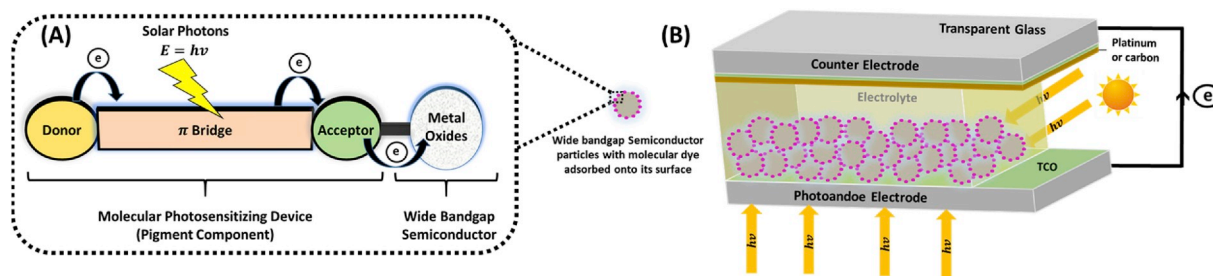
Fig. 1. Schematic Representation of Dye-Sensitized Molecular Device: **(A)** Donor-π-acceptor (D–π–A) structure of an organic dye in DSSCs with a wide bandgap semiconductor photoanode; **(B)** Typical components and architecture including photosensitizer for electron injection, photoanode electrode for charge separation/transport, counter electrode for electron collection, and redox electrolyte for dye neutralization.

when it fulfills these requirements [50]: (i) intense visible-light absorption, (ii) strong chemisorption onto the semiconductor surface, (iii) fast electron injection into the semiconductor CB, and (iv) involve several =O or –OH groups to anchor dye molecules onto the semiconductor surface. The pigment's molecular structure, properties (i.e. hydrophilicity/hydrophobicity, solubility, surface chemistry, and stability of dye molecules), surface morphology, self-assembly, aggregation tendency, anchoring groups, and photosensitizer-electrolyte interactions are some of the basic parameters need to be well understood in order to optimize DSSCs performance through using commercial and/or natural photosensitizers [52]. Uniformly dispersed dyes in an optimal solvent prevent dye agglomeration and enhance dye/semiconductor surface interactions required for the attachment of dye acceptor segments, reducing series resistance and improving electron injection at the interfacial contacts.

Natural dyes extracted from different biological sources (e.g. anthocyanin, carotenoid, flavonoid, aurone, chlorophyll, tannin, and betalain obtained from fruits, flowers, leaves, seeds, barks, and various parts of plants or other biological sources) [61–63] have been proposed to be used as sensitizers in DSSCs due to their low cost and environmental friendliness [50,52,53,64]. Previous studies have mostly investigated on the use of anthocyanins [64,65], flavonoids [66,67], and carotenoids [42] as plant-source photosensitizers. However, Hug et al. (2014) [52] showed that bixin, crocetin, crocin, betaxanthin, betalains, mangostin, rutin, neoxanthin, violaxanthin, and lutein were among the investigated natural sensitizers extracted from plant-based sources. More importantly, anthocyanins (e.g. cyanin and nasunin), anthocyanidin (e.g. delphinidin, cyanidin, and peonidin), chlorophyll (e.g. methyl-3-carboxy-3-devinylpyropheophorbide), and carotenoids (e.g. β-carotene) have been identified as the most promising biomolecular dyes. Carotenoids are highly light-sensitive pigments [39,52] due to their conjugated double π-bonds structure with optimal chain length of seven [68] giving an approximated light-absorption range of 400–500 nm [56,69]. The highest observed performance with single carotenoids in DSSCs was 2.6% [70], where the integration of chlorophyll derivatives with carotenoids can increase the DSSC efficiency up to 4.2% [71]. A major challenge in optimizing DSSC efficiency is the expansion of the absorption range of the photoanode photoactive and/or semiconductor layers [72]. For example, proteins pigment complexes (PPCs) are good alternatives to carotenoids since they have higher absorption coefficient, wider absorbance range (300–1100 nm), and higher conversion efficiency [53,73].

Bacterial pigments have many advantages over the commercial metal-synthetic dyes for DSSCs. Natural pigments from biological sources are promising candidates to be integrated in DSSCs which can be simply installed as rolls in many daily used items such as handbags and clothing as well as building walls, windows and integrated biophotovoltaics [74,75]. Advantages of using natural pigments from biomolecular sources include [53,56,74,75]:

1) Bacteria and their protein complexes and carotenoids are abundant and cost-effective.
2) Extraction of bio-dyes is easy, feasible, and can be also utilized in large scales (scalable).
3) Biological pigments are biodegradable, renewable, and sustainable which makes them very convenient.
4) Pigments from bacterial sources are usually noncarcinogenic and pose no health concerns to humans which makes them environmental-friendly alternatives.
5) Biosensitizers can absorb most of the light energy due to their wide absorption spectrum (multi colors and wavelengths).

Very few works and minimal progress have been devoted towards the use of bacterial protein complexes in bio-sensitized DSSCs which may become a potential alternative as a natural sensitizer. In this context, this review focuses on understanding, analyzing, and exploring available biological pigments extracted from bacteria as potential sensitizers. The aim is to critically evaluate the novelty of utilizing biomolecular bacterial-source pigments as photo-electron sensitizers in DSSCs for solar-to-electricity applications. Several previously designed bio-sensitized DSSC systems have been reviewed, studied, and discussed thoroughly with current knowledge and advancements on the selected biomolecular photosensitizers. Biomolecular pigments discussed in this work include reaction center (RC) proteins [76], chlorophyll a (BChl) [77], chromatophores [45], PPCs including LH2, LH4, and RC; mimicking the principles of natural photosynthesis [78], light-harvesting complex II (LHCII) [79], bacteriorhodopsin (BR) proteins [53,80], xanthophylls carotenoids [56,81], lycopene carotenoids [82], and RC photosystem I trimer (PSI) [83]; where we have studied pigments biological sources, chemical structure, biological information, and their abilities to convert photons-to-electrons in bio-sensitized DSSCs as an attempt to improve the photoelectrochemical performance.

2. Fundamentals of dye-sensitized solar cells

2.1. Architecture

A regular DSSC consists of four important components [49,50,52, 84–86] to initiate the conversion of visible-light photons to electrons. These components and their roles in electron transportation and current generation are briefly: (i) photoanode for charge separation/conduction, (ii) counter electrode for electron collection, (iii) photosensitizer for electron injection, and (iv) redox electrolyte for dye regeneration; as shown in Fig. 1(B). Transparent conductive oxide (TCO) glass substrate sheet resistance of either indium tin oxide (ITO) or fluorine doped tin oxide (FTO) must be low (<15 to 40 $\Omega/\blacksquare$) with a visible-light (400–700 nm) transmission of >80%, facilitating electron injection and transport. Crystallization and annealing of TiO$_2$ film at 100–500 °C are important for better charge transfer and conduction. Covalently bonded dye molecules monolayer to the semiconductor

surface improves photons absorption and e-h pair generation. Dye neutralization occurs *via* liquid or solid (gel) electrolyte when dye molecules receive their missing electrons from reduction of a redox mediator (e.g. iodide and triiodide $[I^-/I_3^-]$ redox couple). A schematic representation of a typical DSSC system with its main components is shown in Fig. 1(B).

2.2. Working mechanism for current generation with possible recombination

The complete operation cycle of DSSCs is composed of four main steps [49,50,59,84,87]:

a) Dye excitation (photonic energy absorption): Dye molecules get excited from their ground state (S) to a higher energy state (S*) with light incident due to photon energy, [from the highest occupied molecular orbital (HOMO) to the lowest unoccupied molecular orbital (LUMO)], and then photon-excited electrons (e-h pairs) are generated.

b) Electron injection (transportation): Excited-dye (S*) is oxidized (S^+) and an electron from S* is injected into the semiconductor CB (e.g. TiO_2); then electrons flow through the porous TiO_2 thin film to the ITO glass substrate where they move from anode to cathode through an external circuit in order to complete the cycle and generate current.

c) Oxidized-Dye regeneration (regeneration): Oxidized-dye (S^+) is regenerated by electron donation from the iodide in the electrolyte and redox mediator $[I^-/I_3^-]$.

d) Electrochemical reduction (cathodic reduction): In return, iodide (I_3^-) in the electrolyte and redox mediator diffuses to the counter electrode (cathode) and gets regenerated by reduction of triiodide ($3I^-$) on the cathode.

There are two recombination mechanisms (e1 and e2) in DSSCs which can be viewed as two competing chemical reactions arise from oxidization of both dye molecules and redox electrolyte species simultaneously [59,87]. Recombination of photogenerated electrons with oxidized dye molecules and/or redox species (I_3^-) takes place within a timescale in microseconds (10^{-6} s) [88,89]. Asbury et al. [90] estimated the time scale for the electron transfer at the semiconductor/dye (injection) and dye/electrolyte (electrolyte reduction) interfaces in 10^{-15} s (femtoseconds) and 10^{-8} s, respectively; which explains the possibility of neglecting recombination from the faster injection mechanism at the semiconductor/dye interface as compared to recombination dynamics from electrolyte reduction (dye/electrolyte) [87]. A schematic representation of the operation cycle and working principle of DSSCs along with both anode and cathode typical redox reactions and recombination dynamics are illustrated in Fig. 2(A–C).

e1) Recombination with the oxidized dye: Arise from loss of excited electrons transferring across the semiconductor/dye interface and/or in the semiconductor which consequently recombine with holes in the oxidized dye (acceptors) in presence of visible-light (photocurrent).

e2) Recombination with the oxidized redox electrolyte: Arise from loss of excited electrons transferring across the dye/electrolyte interface which consequently recombine with holes in the oxidized redox species (I_3^-) in the electrolyte in absence of visible-light (dark current).

2.3. Equivalent circuit model

An equivalent circuit model resembling the simple diode model for DSSCs was proposed by Sarker et al. [91] to relate possible interfacial resistances in DSSCs to the produced cell current and voltage. Total cell current (I_{cell}) may be obtained from applying Kirchhoffs's voltage (KVL) and current (KCL) laws to the circuit model, Fig. 2(D), in order to get Eq. (1) where I_{ph}, I_0, I_r, and I_{sh} refer to cell photo-generated current, dark saturation current, back reaction (recombination) current, and shunt (leakage) current, respectively. Photoanode electrode voltage (V_{PE}) and

I_{sh} are defined in previous works as shown in Eq. (2). Series resistance (R_s), shunt resistance (R_{sh}), recombination resistance (R_r), and applied cell voltage (V_{cell}) in DSSCs play an important role in controlling both V_{PE}, I_{sh}, and therefore I_{cell}. Further, recombination current (I_r) can be determined from Eq. (3) which was obtained from a Boltzmann-like distribution of electrons and V_{PE} that is the difference between electrons Fermi level and electrolyte redox potential. Hence, plugging both Eq. (2) and Eq. (3) in Eq. (1) will yield in Eq. (4) [91] that is the equivalent circuit model for DSSCs; where q (1.602×10^{-18} C) is the electron charge, n is the ideality factor, k_B is Boltzmann constant (1.38×10^{-23} J K^{-1}) and T is the absolute temperature.

$$I_{cell} = I_{ph} + I_0 - I_r - I_{sh} \tag{1}$$

$$V_{PE} = V_{cell} + I_{cell}R_s ; I_{sh} = \frac{V_{PE}}{R_{sh}} \tag{2}$$

$$I_r = I_0 \exp\left(\frac{qV_{PE}}{nk_BT}\right) \tag{3}$$

$$I_{cell} = I_{ph} - I_0\left[\exp\left(\frac{q(V_{cell} + I_{cell}R_s)}{nk_BT}\right) - 1\right] - \frac{V_{cell} + I_{cell}R_s}{R_{sh}} \tag{4}$$

The determined circuit model is comparable to the diode model equation for solar cells as explained in previous literature [92–94]. Both R_s and R_{sh} in DSSCs arise from the interfacial contact resistances between the phase contacts in the compact semiconductor layer [95] influencing electron recombination; Fig. 2(E), specifically at the three interfaces: (i) TiO_2/electrolyte, (ii) TiO_2/dye, and (iii) ITO/electrolyte [85,87,96,97]. Contact and bulk resistances from R_s and defect resistance from R_{sh} are both responsible for increasing recombination rates, shortening electron lifetime, and therefore decreasing the overall cell efficiency.

Eq. (4) can be simplified further to estimate the DSSCs open-circuit voltage (V_{oc}) from the following assumptions [91]: (i) there is an infinite value of R_{sh}, (ii) $I_{cell} = 0$, (iii) $V_{cell} = V_{oc}$, and $(I_{ph} >> I_0) \rightarrow (I_{ph} + I_0 \approx I_{ph})$; which will result in Eq. (5).

$$V_{oc} = \frac{nk_BT}{q} \ln\left(\frac{I_{ph}}{I_0}\right) \tag{5}$$

Similarly, Eq. (4) can be simplified further to estimate the DSSCs short-circuit current (I_{sc}) from the following assumptions [91]: (i) there is an infinite value of R_{sh}, (ii) $I_{cell} = I_{sc}$, (iii) $V_{cell} = 0$, and $(I_{ph} >> I_0) \rightarrow (I_{ph} + I_0 \approx I_{ph})$; which will result in Eq. (6).

$$I_{sc} = I_{ph} - I_0 \exp\left(\frac{qI_{sc}R_s}{nk_BT}\right) \tag{6}$$

For ideal systems: ($R_s \rightarrow 0$); hence, Eq. (6) becomes Eq. (7).

$$I_{sc} = I_{ph} - I_0 \tag{7}$$

3. Bio-photosensitized DSSC for solar-to-electricity conversion

3.1. Sources of biomolecular pigments

Bioactive and/or bio-passive bacterial-based pigments are extracted from complex molecules and small particles found in the cytoplasm of various genetics and living bacterial cells. For example, ribosomes in the bacteria cytoplasm (outside the cell nucleus) is capable of creating different PPCs such that LH2, LH4, and RC as well as producing unique enzymes as hydrogenase for solar-to-energy applications [98–100]. Organic carotenoid pigments (yellow to orange-red) are synthesized by photosynthetic organisms in response to various environmental stresses in many bacteria, algae, fungi, and plants to protect their cells structure from oxidation damage [101–103]. Chlorophyll derivatives synthesized in cyanobacteria, plants, or algae are pigments used to obtain energy from light through photosynthesis [52,61,77]. Various
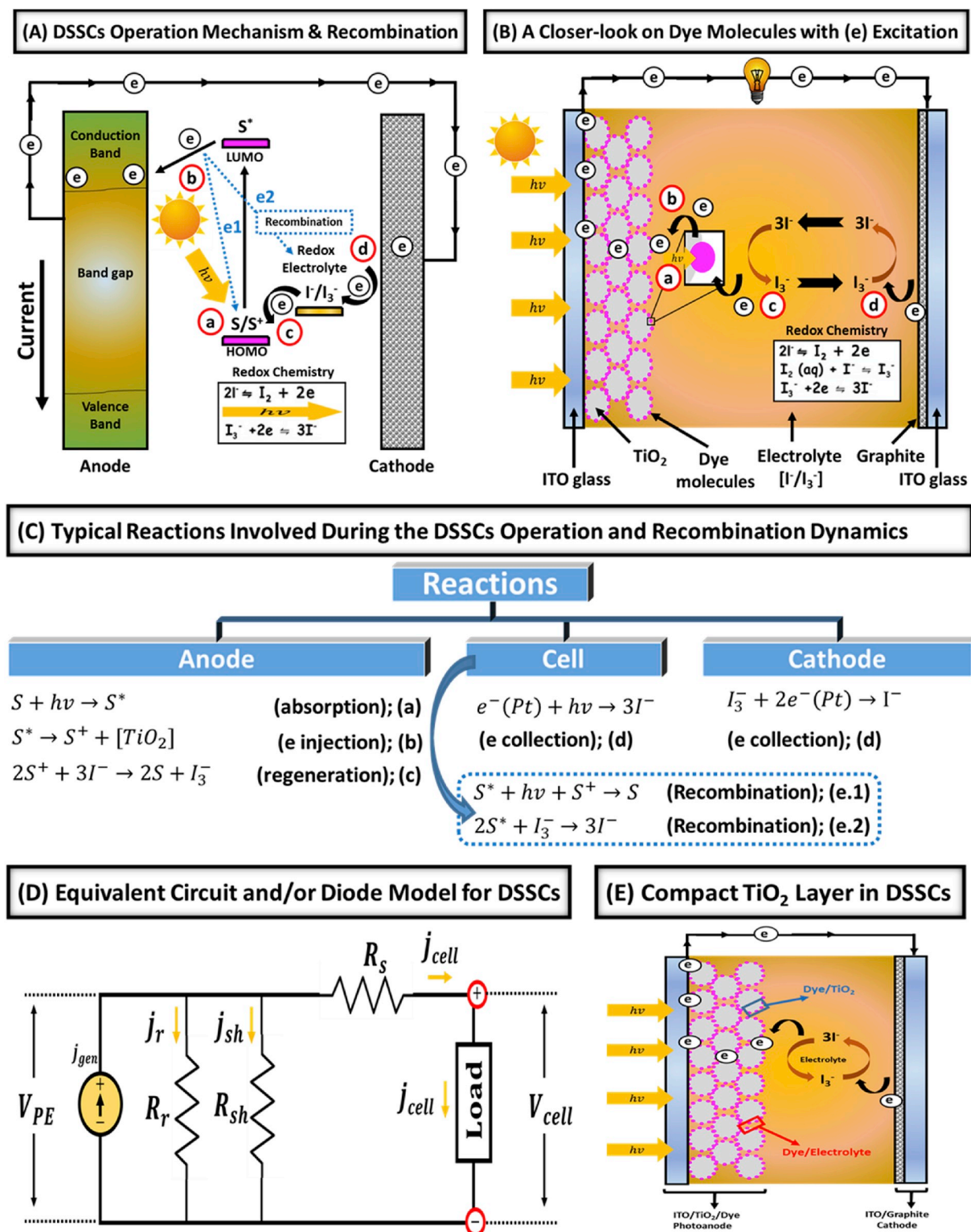
Fig. 2. DSSC Operation Cycle and Reactions: (A) DSSCs complete operation cycle and recombination dynamics; **(B)** Closer-look on the electron excitation and transport in DSSCs; **(C)** Anode (TiO$_2$) and cathode (Pt/C) typical redox reactions in a DSSC (electron flow depends on light intensity and trapping-detrapping effect of the surface); Charge transport/regeneration mechanism in (A) and (B): (a) photons energy excite electrons from HOMO to LUMO levels and generate excitons within the dye molecules to (b) inject excited electron into the conduction band of the semiconductor which initiate charge separation/transport of electrons from photoanode electrode to cathode electrode for current generation while (c) electrolyte ensures continuous current generation by neutralizing dye molecules through (d) redox reactions mechanism, (e1) and (e2) describes possible recombination within DSSCs; **(D)** Diode model for cell (J = I/Area); **(E)** TiO$_2$ photoanode compact layer in DSSCs.

(A) Chlorophyll a derivative (PPB a der.) + Spirilloxanthin (Spx) Carotenoids from Rhodospirillum Rubrum S1

(B) Chromatophores from Rhodospirillum Rubrum S1 + [Quinone (Q0) and cytochrome c] Biological Redox

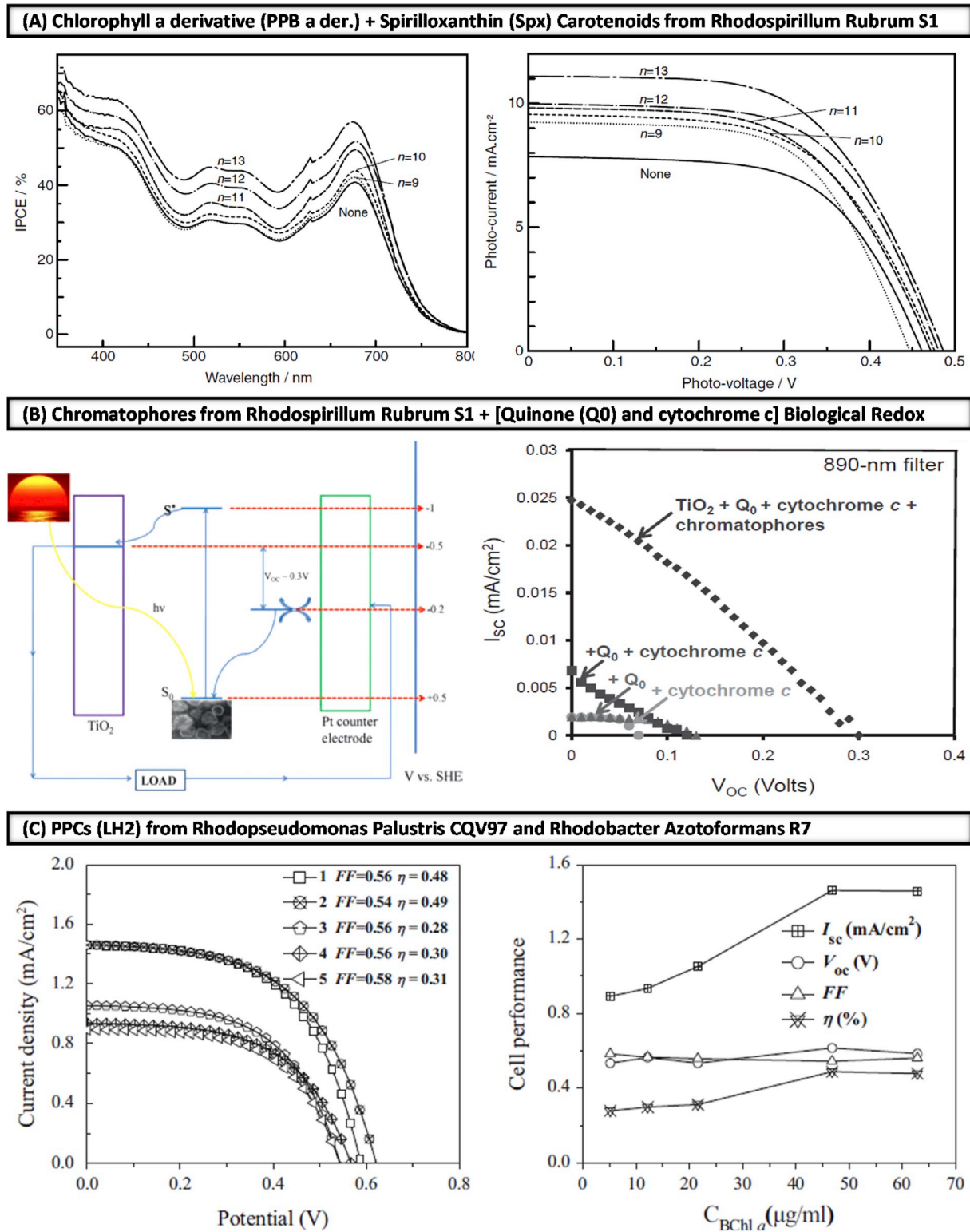**(C) PPCs (LH2) from Rhodopseudomonas Palustris CQV97 and Rhodobacter Azotoformans R7**

Fig. 3. **(A)** IPCE profiles, and I–V curves for the PPB a der. DSSCs without carotenoids and with a 10% each of carotenoids having n = 9–13, Adapted from Ref. [77]; **(B)** Band diagram, and I–V curves of various chromatophores sensitized solar cell (CSSC) under near-IR (NIR) illumination, Adapted from Ref. [45]; **(C)** I–V curves, and photoelectric parameters of DSSCs with different concentrations of LH2, Adapted from Ref. [78].

Table 1
Bacterial sources and chemical structure of various reviewed/discussed bacterial-based biomolecular pigments for bio-sensitized DSSCs.
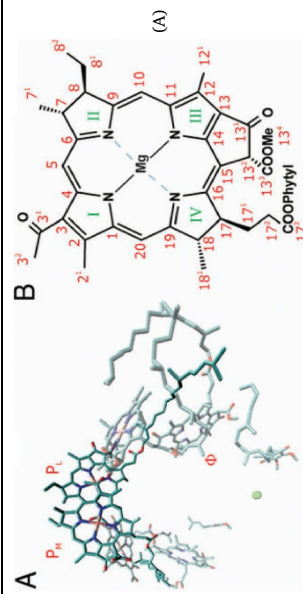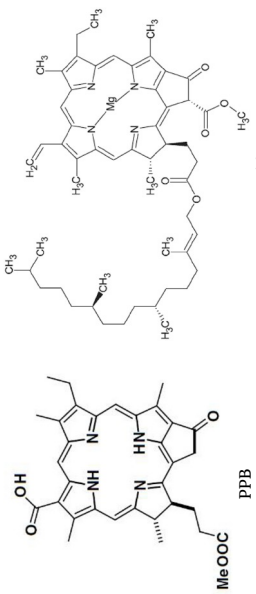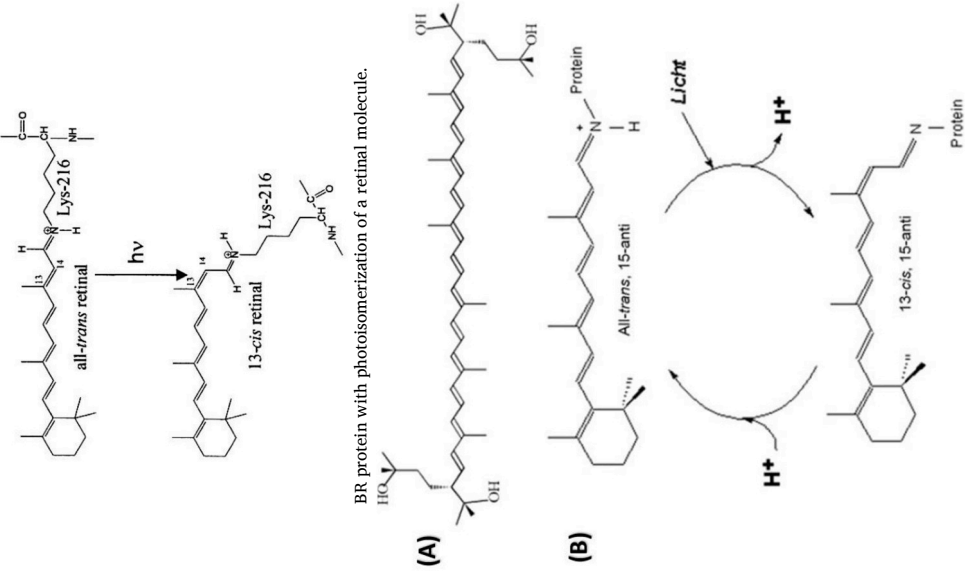
Bio-pigment [Sources]	Chemical Structure/Remark	Ref.
RC Proteins [Rb. sphaeroides (purple non-sulfur bacteria), bacterium RS601 [76] M. pneumoniae, M. genitalium, B. subtilis, S. sanguinis, H. pylori, C. crescentus, P. aeruginosa, and E. coli [110]]	The arrangement of cofactors in the RC of Rb. sphaeroides R26; BChl cofactors, forming the special pair, are labeled as P$_L$ and P$_M$; and (B) BChl a molecule with the numbering of carbon atoms according to IUPAC [111].	[76,110, 111]
Chlorophyll a [Purple bacteria, Heliobacteria, Green sulfur bacteria, Chloroflexi, and Chloracidobacterium thermophilum [112]]	BChl PPB	[52,77, 112]
Carotenoids [Rhodobacter sphaeroides G1C, Rhodobacter sphaeroides 2.4.1, Allochromatium vinosum, and Rhodospirillum rubrum S1 [77]]	Spx	[77]
LH1, LH2, LH3, and LH4 proteins [Purple bacteria, specifically, Rhodopseudomonas palustris CQV97, and Rhodobacter azotoformans R7 [78]]	Love–Hate (LH) ligand structures of LH1. LH2 R= --H LH3 R= LH4 R= Love–Hate (LH) ligand structures 2–4.	[78,113]
Bacteriorhodopsin (BR) protein [Halobacterium salinarum (purple membrane)]		[53,114]

Table 1 (*continued*)

Bio-pigment [Sources]	Chemical Structure/Remark	Ref.
Bacterioruberin (BR) carotenoid [Halobacterium salinarum (purple membrane) [53] and Haloarcula japonica [115]]	BR protein with photoisomerization of a retinal molecule.	[53,115, 116]
Xanthophylls carotenoids [Hymenobacter sp. (red) [56] and Chryseobacterium sp. (yellow) [81] Antarctic bacteria]	(A) Bacterioruberin (BR) carotenoid; and (B) Retinal chromophores of BR in all-trans and 13-cis configurations.	[56,81]

Table 1 (*continued*)
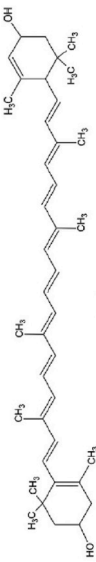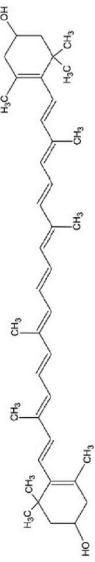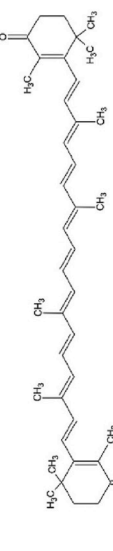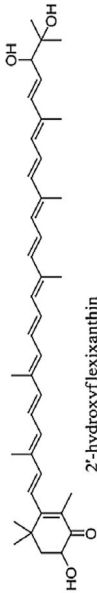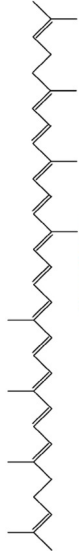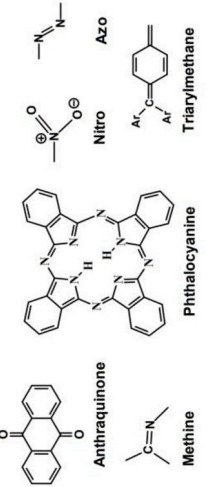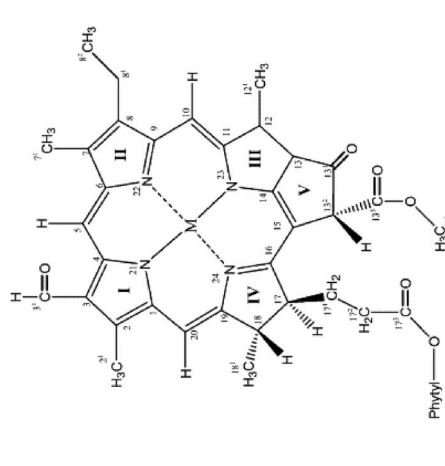
Bio-pigment [Sources]	Chemical Structure/Remark	Ref.
Xanthophylls pigments [Hymenobacter sp. (red) [56], and Chryseobacterium sp. (yellow) [81]]	Lutein Zeoxanthin Canthaxanthin	[56,81]
Lycopene carotenoids [*E. coli* [82]]	2'-hydroxyflexixanthin RAW orange from Antarctica bacteria Lycopene	[82,117]
Chromatophores [Rhodospirillum rubrum [45] and Rhodobacter sphaeroides [118]]	Anthraquinone Nitro Azo Methine Phthalocyanine Triarylmethane Examples of chromophoric groups present in organic dyes [119].	[45,118, 119]
RC photosystem I trimer (PSI) [Cyanobacteria and/or thermophilic cyanobacteria Thermosynechococcus elongatus]		[83,120]

9

Table 1 (*continued*)

Bio-pigment [Sources]	Chemical Structure/Remark	Ref.
	A trimeric PSI complex isolated from *A. marina* contains ~180 Chl d molecules with carbonyls [120].	

reviewed/discussed bacterial-based biomolecular pigments for bio-sensitized DSSCs are shown in Table 1.

3.2. Chemical structure of biomolecular pigments

The chemical structure and structural remarks of the studied biomolecular pigments for bio-sensitized DSSCs from different bio-pigment categories (e.g. proteins, carotenoids, and chlorophyll) are shown in Table 1. Available functional groups, chemical (covalent) and physical bonds, number of conjugated double π-bonds (n), and length of the organic hydrocarbon structure chain are some of the parameters that should be considered in the selection of an ideal bio-pigment for DSSCs. Hydrocarbon chains with lots of hydroxylic (–OH), carboxylic (–COOH), and (=O) radicals are preferred for strong binding and attachment of dye molecules onto the semiconductor surface resulting in lower electron resistance and facilitated electron injection [77,104]. Shahzada et al. [105] reported on the possibility of incorporation of phenyl units on both the donor and acceptor moieties within the dyes (e.g. phenyl-alkoxy substituted triphenylamine donor based sensitizers) which can effectively reduce recombination and aggregation to give higher power conversion. Cui et al. [106] determined that the introduction of bulky groups (e.g. alkyl chains or aromatic rings) in the pigment's spacer segment may also inhibit dye aggregation and increase electron lifetime.

Conjugated systems such as carotenoids show strong colors or pigments due to the presence of conjugated electrons in their structure. Free π-electrons arise from the conjugated double bonds structure describes alternation between single and double bonds in the long hydrocarbon chains. The conjugated π-bonds result in the strong carotenoids colors and their light-absorption properties allowing current generation from easy photoexcitation of free electron carriers reside along the molecular chain. Photoexcitation initiates electron transition to a higher energy level from an even-symmetry conjugated π-system molecular orbital to an odd-symmetry molecular orbital (π to π^*). Typically, an electron transient with photoexcitation from HOMO level to LUMO level according to the selection rules for electromagnetic transitions. Pigments from carotenoids only show up when the number of conjugated double bonds is (n > 8) and that system with few conjugations (n < 8) only absorbs strong light energy like UV radiations. Visible-light energy (low energy) can be absorbed by carotenoids constituents that have enough conjugated double bonds (n > 11) which typically observed as orange to red pigments. In other words, molecules with more conjugated bonds absorb lower energies of light than molecules with fewer conjugated bonds [107–109]. Functional groups, conjugated bonds, and other bonds within the chemically structured long hydrocarbon chains of the reviewed/discussed bacterial-based biomolecular pigments for bio-sensitized DSSCs are illustrated in Table 1.

4. Current advancements in bio-sensitized DSSCs

Photosynthetic RC proteins consist of a transmembrane pigment-protein complex across the bacteria which act as a charge separator of the photo-formed e-h pairs [76]. Semiconductor/protein films and their functionalization have been recently extensively studied due to their promising role in the development of bioelectronics and bio-photoelectric devices [76,121,122]. Yet, researchers are still unable to overcome two major problems: (i) loss of energy due to the formation of the final charge separation state of RC [123,124], and (ii) charge recombination of the photoinduced electrons which hinders separation of e-h pairs that greatly hamper the photoelectric conversion of such RC [76]. A new type of bio-sensitized DSSCs known as photosynthesis DSSCs, which is based on the principle and materials of photosynthesis, has gained much attention from the scientific community for photovoltaic applications [104]. Chlorophyll derivatives are considered as a great biological alternative for traditional dye sensitizers in DSSCs for

Table 2

Performance comparison of bio-sensitized DSSCs according to the used dyes or various reviewed and discussed bacterial-based biological pigments for solar-to-electricity generation.

Bacterial Pigment	Remarks: Structure/Electrolyte and Irradiation/Absorption	J_{sc} (μA cm^{-2})	V_{oc} (mV)	FF	η[b] (%)	Ref.
Chlorophyll a (PPB)[a] + Carotenoids (Spx)[a]	FTO/TiO$_2$/PPB/carotenoids/Electrolyte/Pt/FTO; Electrolyte: Methoxyacetonitrile solution containing 0.1 M LiI, 0.05 M I$_2$ and 0.6 M 1,2-dimethyl-3-propyl-imidazolium iodide (DMPI); Irradiation: 300 W/100 mW cm^{-2} (AM1.5); PPB combined with 10% of Spirilloxanthin (Spx) as carotenoids; Absorbance: max @ 680 nm; Absorption spectra: 400–600 nm.	11500	–	–	4	[77]
Chromatophores	FTO/TiO$_2$/chromatophores/Teflon + Electrolyte/Pt/FTO; Electrolyte: quinone (Q0) + cytochrome c; Irradiation: 890 nm light; No external voltage; Absorption peaks: 485, 550, 590, 520, 805, and 880 nm from carotenoids and monomeric BChl of the RC; Absorption spectra: 430–900 nm.	24.7	300	0.29	0.04	[45]
PPCs (LH2)[a]	FTO/TiO$_2$/PPCs/Electrolyte/Pt/FTO; Electrolyte: 0.5 M LiI, 0.05 M I$_2$, 0.3 M DMPII, 0.5 M 4-TBP and 0.1 M GNCS in acetonitrile; LH2-sensitized with a concentration of 46.8 μg BChl mL^{-1} on TiO$_2$ film; Absorbance: max @ 803 and 856 nm for P-LH2, 802 and 847 nm for P-LH4 from strain CQV97; Absorption spectra: 600–900 nm.	1460	620	0.54	0.49	[78]
PPCs (RC)[a]	Structure/Electrolyte and Irradiation/Absorption as PPCs (LH2); RC-sensitized.	1240	840	0.55	0.57	[78]
Light-harvesting complex II (LHCII)[a]	Structure/Electrolyte and Irradiation/Absorption as PPCs (LH2); LHCII-sensitized.	800	590	0.58	0.27	[79]
Bacteriorhodopsin proteins and bacterioruberin carotenoids (BRs)[a]	FTO/TiO$_2$/bacteriorhodopsin/bacterioruberin/electrolyte/Pt/FTO; Electrolyte: N/A; Irradiation: 100 mW cm^{-2} (AM1.5); Absorbance: max @ 568 nm for bR and @ 497 nm for Bacterioruberin; Absorption spectra: 300–650 nm.	450	570	0.62	0.16	[53]
Xanthophylls carotenoids (yellow)[a]	FTO/TiO$_2$/xanthophylls/electrolyte/Pt/FTO; Electrolyte: iodide/triiodide [I^-/I_3^-]; Irradiation: 100 mW cm^{-2} (AM1.5); yellow pigments were isolated from chryseobacterium sp.; Absorbance: max @ 450 and 490 nm (close to β-carotene @ 400 and 550 nm); Absorption spectra: 300–600 nm.	130	549	–	0.0323	[56]
Xanthophylls carotenoids (red)[a]	FTO/TiO$_2$/xanthophylls/electrolyte/Pt/FTO;Electrolyte: iodide/triiodide [I^-/I_3^-]; Irradiation: 100 mW cm^{-2} (AM1.5); red pigments were isolated from hymenobacter sp.; Absorbance: max @ 490 and 520 nm (slightly shifted to longer wavelengths); Absorption spectra: 300–600 nm.	200	435	–	0.0332	[56]
Xanthophylls carotenoids (PURE orange)[a]	FTO/TiO$_2$/xanthophylls/electrolyte/Pt/FTO; Electrolyte: iodide/tri-iodide [I^-/I_3^-] in acetonitrile; Irradiation: 100 mW cm^{-2} (AM1.5); (PURE orange)-sensitized; Absorbance: N/A; Absorption spectra: N/A.	78	260	0.39	0.008	[81]
Xanthophylls carotenoids (RAW orange)[a]	Structure/Electrolyte and Irradiation as xanthophylls carotenoids (PURE orange); (RAW orange)-sensitized; Absorbance: N/A; Absorption spectra: N/A.	127	460	0.51	0.03	[81]
Xanthophylls carotenoids (Cocktail)[a]	Structure/Electrolyte and Irradiation as Xanthophylls carotenoids (PURE orange); Cocktail-sensitized; Absorbance: N/A; Absorption spectra: N/A.	98	260	0.38	0.009	[81]
Lycopene carotenoids	FTO/TiO$_2$/E. coli (lycopene)/Electrolyte/C/FTO; Electrolyte: [I^-/I_3^-]; Irradiation: 100 mW cm^{-2} (AM1.5); Absorption peaks: 450, 475, and 505 nm; Absorption spectra: 350–750 nm.	696	289	–	0.057	[82]
RC photosystem I trimer (PSI)[a]	FTO + ITO/TiO$_2$+ZnO/PSI/Pt + glass; Electrolyte: Z813 Co(II)/Co(III); Irradiation: 100 mW cm^{-2} (AM1.5); Absorption peaks: 800 nm; Absorption spectra: N/A.	362	500	0.71	0.08	[83]
Bacteriorhodopsin (BR)[a] protein	FTO/TiO$_2$/BR/Electrolyte/Pt/glass; Electrolyte: [I^-/I_3^-] which is a liquid electrolyte; Irradiation: 100 mW cm^{-2} (AM1.5); Absorption peaks: N/A; Absorption spectra: N/A.	620	–	–	0.19	[80]
Bacteriorhodopsin (BR)[a] protein	FTO/TiO$_2$/BR/Electrolyte/Pt/glass; Electrolyte: acetamide based gel electrolyte modified poly(ethylene)oxide (PEO); Irradiation: 100 mW cm^{-2} (AM1.5); Absorption peaks: N/A; Absorption spectra: N/A.	1008	–	–	0.49	[80]

[a] Meaning of symbols in parenthesis and their definitions can be found in the subheadings of section 4, or from Figures 3 and 4.
[b] Efficiency = Incident photon-to-current efficiency (IPCE) = Quantum efficiency (QE).

the conversion of solar energy to electricity [77]. The blending of chlorophyll with photosynthetic pigments like carotenoids has shown much improvements and developments in chlorophyll sensitizing function in DSSCs since carotenoids play a key role in harvesting light energy, protecting chlorophyll layer [125,126], and forming radical cations for the redox function [127].

A) Chlorophyll a derivative (PPB a der.) + Spirilloxanthin (Spx) Carotenoids from Rhodospirillum Rubrum S1: In a recent work, Wang et al. [77] utilized chlorophyll a derivative (methyl 3-carboxy-3--devinyl-pyropheophorbide a; abbreviated as PPB a der.) as a photosensitizer in DSSC which was also combined with 10% of different conjugation lengths of carotenoids as redox spacers. Chlorophyll a (PPB a der.) bio-sensitizer consists of a chlorine skeleton which contains a carboxyl group that is directly attached to the conjugated macrocycle (Table 1). Carboxyl groups enhance binding and/or attachment of chlorophyll a onto the surface of the used semiconductor materials in DSSCs such as TiO$_2$. This firm attachment can effectively facilitate electron transport and injection from chlorophyll a/carotenoids into TiO$_2$ nanoparticles [77,104]. The addition of biological carotenoids and

conjugated spacers (e.g. spinach reaction centers and/or spirilloxanthin (Spx) from rhodospirillum rubrum S1) would also improve electron transfer through: (i) neutralizing the dye molecules, and (ii) blocking reversed electrons from being oxidized by the formation of radical cations which aid in redox reactions [77,127]. Wang et al. [77] constructed his biologically-sensitized DSSC as the following [FTO/TiO$_2$/PPB/carotenoids/Electrolyte/Pt/FTO] with the use of methoxyacetonitrile electrolyte solution for the redox function and 10% of Spx as carotenoids isolated from rhodospirillum rubrum S1. The bio-sensitized DSSC was irradiated with a halogen lamp of 100 mW cm^{-2} for photoelectrical analysis of short-circuit current density (J_{sc}) and conversion efficiency, which were determined to be 11.5 mA cm^{-2} and 4.0%, respectively (Table 2). The mechanism of the electron transfer to the dye from the redox function of carotenoids involves: (i) PPB a der. excitation from photon absorption, (ii) exciton generation from the PPB a der. (dye) molecules which is maintained/facilitated from carotenoids redox role in generating carotenoids radical cations, (iii) electron injection into TiO$_2$ CB for a charge-separation state between dye radical cations and electrons, and (iv) reverse electron transfer which may occur and result
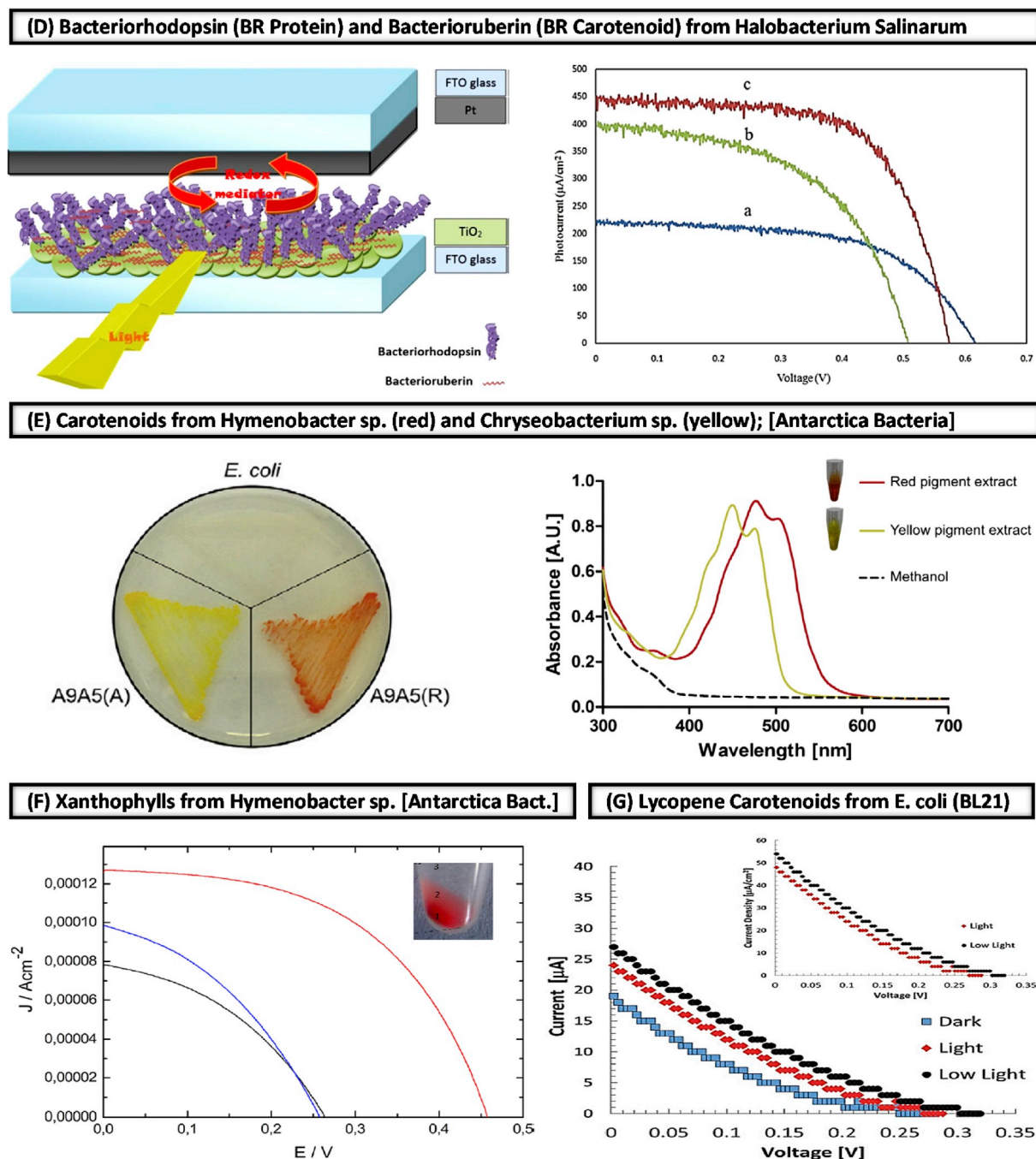
Fig. 4. (D) Bio-sensitized DSSC system, and I–V curves for the DSSC sensitized with (a) Bacterioruberin (BR carotenoid), (b) Bacteriorhodopsin (BR protein), and (c) a mixture of two pigments, Adapted from Ref. [53]; **(E)** Agar plate with pigmented A9A5(R) and A9A5(A) isolates, for the yellow and red pigments, respectively, and *E. coli* as non-pigmented bacteria, with visible-light absorbance of yellow and red pigments, Adapted from Ref. [56]; **(F)** I–V curves for the bio-sensitized DSSCs using different pigments: PURE orange (black line), RAW orange (red line) and cocktail orange + co-adsorbent (blue line), inset: extracted dye from centrifuge with numbers as (1) bacterial pellet, (2) slime, (3) supernatant, Adapted and modified from Ref. [81]; **(G)** I–V curves of the bio-PV DSSC using *E. coli*/lycopene as a biological sensitizer, Adapted from Ref. [82]. (For interpretation of the references to color in this figure legend, the reader is referred to the Web version of this article.)

in charge recombination that will lower current production [77]. The IPCE profiles and I–V curves observed from Wang et al. experiments [77], as shown in Fig. 3(A), concluded that both efficiency and current increase as linear functions of n (numbers of conjugated double bonds; n = 9–13) due to the described electron-transfer mechanism.

B) Chromatophores from Rhodospirillum Rubrum S1 + [Quinone (Q0) and cytochrome c] Biological Redox: Another study on biohybrid photovoltaics by Magis et al. [118] assessed the use of both bio-sensitizers and bioelectrolytes as bacterial photosynthetic membrane vesicles (chromatophores adsorbed to a gold electrode). Chromatophores from rhodospirillum rubrum together with Q and cytochrome c as electrolytes were used in a designed biohybrid cell to collect light energy from both blue light and near-IR photons (800–875 nm). The absorbed energy is then transferred into the RC bacteriochlorophyll a (BChl) special pair to initiate charge separation within chromatophores which will consequently facilitate the unidirectional flow of electrons from the provided band energies between consecutive interfaces. The light-driven current generation was found to be dependent

on: (i) the biological/bare gold electrode, (ii) the electrolytes, and (iii) the open circuit potential of 100 mV; which was capable of achieving a high J_{sc} of 25 µA cm^{-2}.

Woronowicz et al. [45] developed a biohybrid DSSC known as chromatophores sensitized solar cell (CSSC) where the organic light-harvesting dye was replaced with chromatophores isolated from rhodospirillum rubrum strain S1 and regular electrolyte (I^- / I_3^-) was substituted with biological electrolytes (redox mediators of biological origin) as quinone (Q0) and cytochrome c. It was found that the CSSC with the configuration [FTO/TiO$_2$/chromatophores/Teflon+Electrolyte /Pt/FTO] showed a higher performance, Fig. 3(B) and Table 2, under AM1.5 (890 nm) due to the good CSSC capability in utilizing both visible and near-IR irradiation, generating light-induced current and tunneling electrons to the TiO$_2$ through the biological redox mediators. The CSSC system was tested with a dark current for recombination evaluation of (TiO$_2$ + chromatophores + Q0 + cytochrome c) which showed the least e-h recombination in the TiO$_2$ CB, because of the attachment of chromatophores on the semiconductor electrode (TiO$_2$ surface) that act as a barrier layer between electrons and holes in both TiO$_2$ CB and the electrolyte Q0/cytochrome c. A unidirectional flow of electrons within the biological dye was observed due to the significant reduction in back transfer rate from the good coupling between utilized biological components (electrode and electrolyte) and from the excellent band energy agreement between consecutive interfaces.

C) PPCs (LH2) from Rhodopseudomonas Palustris CQV97 and Rhodobacter Azotoformans R7: Fu et al. [78] have been able to incorporate bio-pigments from protein complexes (PPCs as LH2, LH4, and RC) into a TiO$_2$ film for the fabrication of a promising biological photoanode sensitizer for visible-NIR responsive DSSCs with the configuration [FTO/TiO$_2$/PPC/Electrolyte/Pt/FTO] [79]. PPCs were isolated and extracted from purple bacteria (rhodopseudomonas palustris CQV97 and rhodobacter azotoformans R7). LH2-sensitized DSSCs were capable of producing high photocurrents reported to be stable for several working cycles (on/off settings) for more than 300 s. The I–V test was carried out under 100 mW cm^{-2} to identify the effect of the different PPCs absorption bands (750–850 nm) on J_{sc} and PCE. Photoelectric performance of the designed bio-sensitized DSSCs was enhanced with the increase in LH2 concentrations and with a negligible decay at zero bias voltage. The optimal concentration of 46.8 µg BChl mL^{-1} of LH2 on TiO$_2$ film (72 h absorption) has been identified to have the maximum J_{sc} and η as 1.46 mA cm^{-2} and 0.49%, respectively, (Fig. 3(C) and Table 2). However, LH2 concentrations showed no apparent effect on both V_{oc} and FF parameters and that RC-sensitized DSSCs had better electric properties than LH2 due to its efficient charge separation which allows the photoanode to transfer electrons much faster from light-sensitization, completing the circuit for efficient light-electric conversion. The response of PPCs-sensitized TiO$_2$ film became more prominent to visible-NIR light energy which advanced electron transfer from PPCs into TiO$_2$ CB to successfully produce current from the designed bio-sensitized DSSCs based on purple bacterial PPCs [78].

D) Bacteriorhodopsin (BR Protein) and Bacterioruberin (BR Carotenoid) from Halobacterium Salinarum: Molaeirad et al. [53]
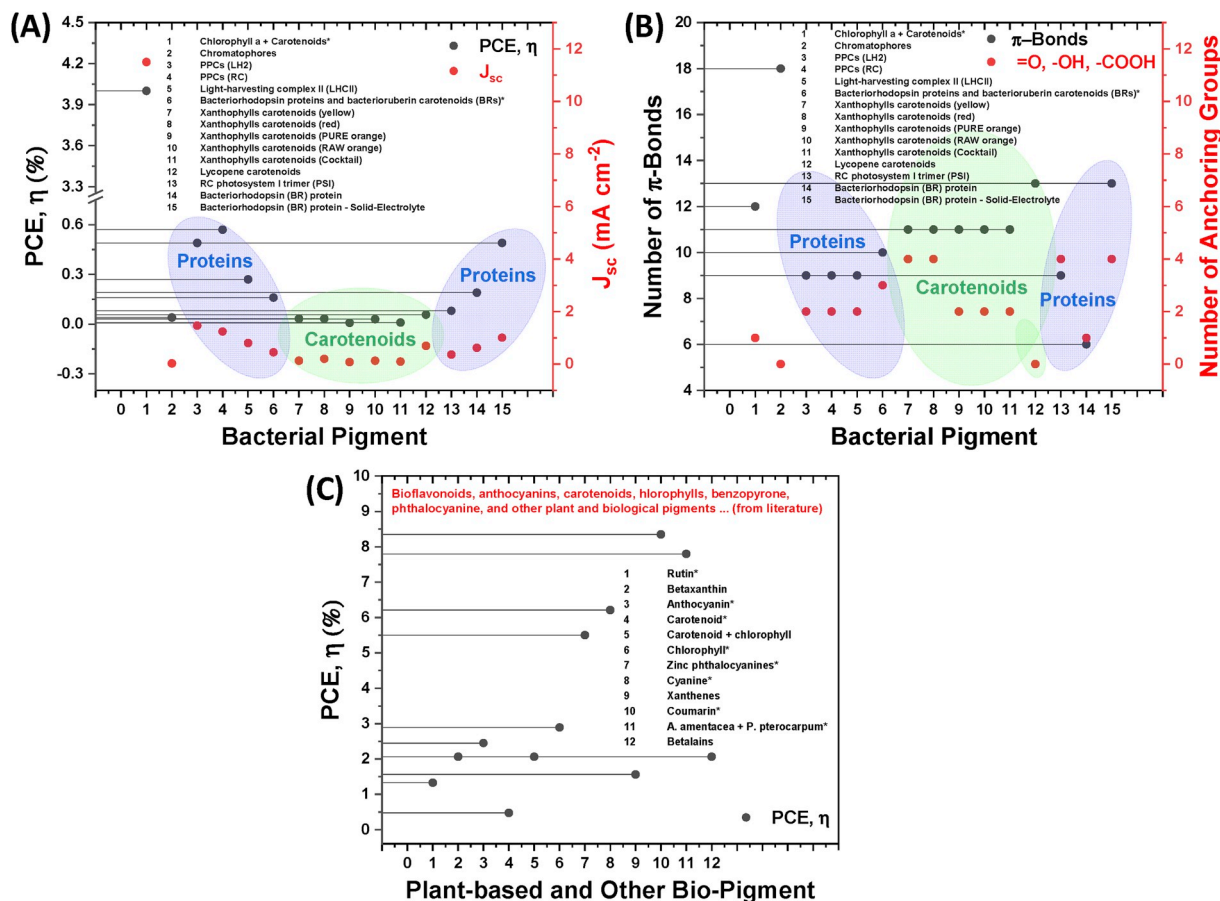

Fig. 5. Statistical plots relating bio-sensitized DSSCs performance to the studied bacterial-based pigments (e.g. proteins and carotenoids), Ref. [45,53,56, 77–83], **and their bio information and molecular structures: (A)** DSSC power conversion efficiency (PCE) and short-circuit current density (J_{sc}); **(B)** Number of existing conjugated double π-bonds and acceptor-segment anchoring groups in a dye molecule. **(C)** Other highly-efficient literature reviewed plant-based and biological pigment classes, Ref. [50,138–147], utilized in bio-sensitized DSSCs for comparisons. Note: asterisk (*) indicates PCEs were averaged to the higher integer based on different literature data from Ref. [45,50,53,56,77–83,138–147], electrolyte in **(A)** and **(B)** is I/I$_3$ except for pigments (2,13,15) with solid-state or other redox electrolyte.

investigated on the use of another inexpensive class of bacterial pigments as sensitizers in DSSCs, knowns as (BR), from bacteriorhodopsin and bacterioruberin which are natural-colored biomolecules of proteins and carotenoids, respectively, and usually found in the cytoplasmic membrane of halobacterium salinarum. Bacteriorhodopsin (BR) protein consists of 248 amino acids arranged inside the lipid membrane in seven α-helical bundles; upon photon absorption, absorbed energy initiates retinal isomerization (Table 1) to convert all-trans BR to the 13-cis configuration which therefore triggers the photocycle by transferring one proton from the cytoplasmic to the extracellular side of the membrane [128,129]. On the other hand, bacterioruberin (BR) carotenoid contains 50-carbon open-chain with 13 pairs of conjugated double bonds which effectively contribute in involving hydroxyl free-radicals for photoprotection [130]. Molecular structures of both described BRs can be found in Table 1.

Molaeirad et al. [53] have sensitized different TiO_2 electrodes through immersion in a solution of 1.5 mL containing 1 mg mL^{-1} bacteriorhodopsin and 0.1 M bacterioruberin, separately, for 12 h at room temperature [131]. Upon simultaneous adsorption, TiO_2 films were observed in purple and red colors indicating the binding and attachment of BR biomolecules on the nano-TiO_2 surface. The bio-pigment-coated TiO_2 films were tested in DSSCs with the configuration [FTO/TiO_2/-bacteriorhodopsin/bacterioruberin/Electrolyte/Pt/FTO] and with hot-melt Surlyn film (30 μm) as a spacer between electrodes. Under 100 mW cm^{-2} (AM1.5) irradiation, a maximum cell efficiency of 0.16% was observed when using both pigments simultaneously (Fig. 4(D) and Table 2); which provided much better performance than using the two pigments separately. The combination of the two pigments allowed for more sensitization of the TiO_2 films and expanded the light-absorption spectrum (broad range of wavelengths) with a maximum visible-light absorbance at 568 nm and 497 nm for bacteriorhodopsin and bacterioruberin, respectively [53].

E) Carotenoids from Hymenobacter sp. (red) and Chryseobacterium sp. (yellow); [Antarctica Bacteria]: Órdenes-Aenishanslins et al. [56], in their recent work (2016) and for the first time, utilized non-photosynthetic UV-resistant Antarctic bacteria for the production of pigments utilized as photosensitizers in DSSCs. It was discovered that bacteria living in the Antarctic region developed a mechanism to resist UV-damage by improving their DNA structure [132, 133] to synthesize carotenoid pigments which act as antioxidants, that protect bacteria structure against oxidative stress [134] and tolerate excessive UV irradiation [135]. The bacteria were first isolated from the collected soils of King George Island, Antarctica, and then incubated, purified, and centrifuged to obtain the red and yellow pigments which were later classified as carotenoids and identified as hymenobacter sp. (red) and chryseobacterium sp. (yellow) bacteria as shown in Fig. 4(E). A TiO_2 film was sensitized with both pigments, separately, by direct adsorption (twice) in a pigment solution of 10 mg mL^{-1} incubated in darkness. Both pigments were characterized for their maximum visible-light absorbance and the peaks were found at 450 nm and 478 nm for the yellow and red pigments, respectively.

The sensitizing performance of both xanthophylls pigments (carotenoids) was evaluated in a fabricated DSSC with the structure [FTO/TiO_2/xanthophylls/(I^-/I_3^-)/Pt/FTO] and under solar radiation of 100 mW cm^{-2} (AM1.5). The determined DSSCs efficiencies were 0.0323% and 0.0332% for the yellow-pigment DSSC and red-pigment DSSC, respectively (Table 2). The photostability of the isolated carotenoids was investigated from the decay in light absorbance at different exposure times, and it was evident that the UV-resistant carotenoids are quite stable under light exposure for long times [56].

F) Xanthophylls from Hymenobacter sp. [Antarctica Bacteria]: Montagni et al. [81] also utilized xanthophylls pigments as sensitizers in DSSC which were extracted from hymenobacter sp. UV11 bacteria collected from Antarctica. It was hypothesized that Antarctic bacteria evolved to produce these kinds of pigments for light energy harvesting even under non-direct sunlight conditions. The use of co-adsorbents as

co-adsorbents (polysaccharides as α-1,4-glucan) with bacterial dyes was investigated as an attempt to increase DSSC conversion efficiency. Three different xanthophylls dye solutions: (i) RAW orange, (ii) PURE orange, and (iii) a mixture of PURE orange plus chenodeoxycholic acid (cocktail) were used for overnight sensitization of the photoanode [FTO/TiO_2]. RAW orange dye was purified using pre-purchased disposable silica columns. The three dyes were tested in a DSSC with the configuration [FTO/TiO_2/xanthophylls/Electrolyte/Pt/FTO] to determine the performance IV curves, as shown in Fig. 4(F), where the test was carried with 50 mM iodide/tri-iodide in acetonitrile electrolyte with a solar radiation of 100 mW cm^{-2} (1 sun) and AM1.5. The highest conversion efficiency (0.03%) was observed for the RAW orange-xanthophylls pigment (Table 2) due to the presence of the unpurified polysaccharides co-adsorbent (α-1,4-glucan) which might have helped in improving bonding/anchoring of xanthophylls pigments onto the TiO_2 surface because of the extra available OH groups. Red/orange-xanthophylls pigments from hymenobacter sp. UV11 along with their polysaccharides co-adsorbents might become a promising biological sensitization option in DSSCs to increase the conversion efficiency.

G) Lycopene Carotenoids from E. coli (BL21): A genetically engineered *E. coli* has been developed to produce the photoactive pigment lycopene as a biogenic material for photovoltaic applications [82]. Lycopene is a natural type of carotenoids which gives tomatoes and/or some bacteria their orange-red pigmented colors. Lycopene pigments are stable redox mediators that absorb light energy in the range of 380–520 nm and efficiently excites HOMO-electrons; hence, used as a photosensitizer in PV and photocatalytic applications [61, 136]. Srivastava et al. [82] encapsulated a porous mesh of *E. coli* (BL21) cells with TiO_2 nanoparticles *via* a tryptophan-mediated supramolecular interface in order to produce a core@shell-like morphology of TiO_2/*E. coli*/lycopene for DSSC applications. The obtained biogenic photovoltaic composite was then coated onto an FTO glass and tested for its photovoltaic performance under a solar simulator (100 mW cm^{-2} and AM1.5) in a DSSC configuration [FTO/TiO_2/lycopene/Electrolyte/C/FTO] with the redox electrolyte [I^-/I_3^-]. It was evident from the IV curves from Fig. 4(G) that *E. coli*/lycopene had an absorbance maxima in the visible region at 450, 485, and 595 nm which yield in 0.057% PCE (Table 2) with a great conversion feasibility at both high-light and low-light intensities under ambient conditions [82,137].

Previously designed bio-sensitized DSSCs were critically reviewed for their photo-electric conversion effectiveness as shown in Table 2. Bio-pigments extracted from protein complexes (LH2, BR, RC) and chlorophyll a derivatives combined with carotenoids showed the highest bio-sensitized DSSCs performance, among the studied dyes, for solar-to-electricity applications with a conversion efficiency of 0.16–0.57%, and 4%, respectively. Conversely, xanthophylls carotenoids isolated from Antarctic bacteria reserved the lowest photoelectric conversion performance of 0.008–0.03% in comparison with other studied biomolecular pigments, where the use of co-adsorbents boosted up the performance to 0.03% due to dye strong anchoring capabilities for enhanced charge carriers transport and electron injection.

Under 1 sun radiation (100 mW cm^{-2}), the authors critically analyzed reported photovoltaic parameters of other plant-based biomolecular photosensitizers to estimate and/or report the DSSCs performance attributed to using: mangosteen pericarp (rutin) 1.17% [50], rhoeo spathacea (rutin) 1.49% [138], sicilian prickly pear (betaxanthin) 2.06% [139], black rice (anthocyanin) 3.27% [140], capsicum (carotenoid) 0.58% [140], erythrina variegata flower (carotenoid, chlorophyll) 2.06% [140], rosa xanthine (anthocyanin) 1.63% [140], kelp (chlorophyll) 1.18% [140], organic dye zinc phthalocyanines 4.6% [141] and 6.4% [142], cyanine dyes 4.8% [143] and 7.62% [144], rose bengal (xanthenes) in ZnO-based DSSCs 1.56% [145], coumarin dyes having thiophene moieties in TiO_2-based DSSCs 7.7% [146] and 9% [147].

More recent review studies (2015–2019) showed the promising role of biomolecular sensitizers for the development of bio-sensitized DSSCs.

Table 3
Isolation/extraction processes adopted in extracting bacterial-based pigments from various reviewed and discussed biomolecules for solar-to-electricity bio-sensitized DSSCs.

Bacterial Pigment	Remarks on Bacteria Isolation and Pigment Extraction	η (%)	Ref.
Chlorophyll a (PPB) + Carotenoids (Spx)	Spirilloxanthin (Spx) was isolated from rhodospirillum rubrum S1. bacteriochlorophyll and lipids were removed by washing cells with methanol, centrifuged, washed with acetone, and centrifuged again. Resultant cells were washed with benzene and centrifuged (3 times) to completely extract the carotenoids after fractionating benzene solution against NaCl aqueous. Benzene layer containing carotenoids was filtered using low-pressure liquid chromatograph.	4	[77, 167]
Chromatophores	Cell growth was done by keeping Rsp. rubrum strain S1 to grow for 3 days under 1-sun condition and at 30 °C. Chromatophores were isolated from French pressure through rate-zone sedimentation on sucrose density gradients, then isolated mixture was centrifuged and resuspended in 0.1 M Na$_2$PO$_4$. Purified membrane (lipid) fractions were obtained from trichloroacetic acid-precipitated by two chloroform-methanol extractions.	0.04	[45]
PPCs (LH2)	Bacterial PPCs were isolated from collected sand using StrainCQV97 and R7 cultured anaerobically in modified Ormerod medium at 30 °C for 1 h, then PPCs were purified with ammonium-sulfate fractionation (DEAE-52 anion-exchange) and gel-filtration chromatography.	0.49	[78]
PPCs (RC)	Pigment Extraction as PPCs (LH2).	0.57	[78]
Bacteriorhodopsin proteins and bacterioruberin carotenoids (BRs)	Two strains of H. salinarum, NRC-1 and R1, were used for extraction of bacteriorhodopsin and bacterioruberin, respectively. Strain cells were ground with quartz powder, extracted with ethanol, ether, and 15% NaCl aqueous solution to separate organics. The organic layer was dried over anhydrous sodium sulfate, loaded with a benzene solution on a silica gel column. Bacterioruberin pigments were diluted with acetone:benzene (42:58), pooled and concentrated under reduced pressure. The bacterioruberin was dissolved in acetone and stored under N$_2$ gas in the dark at −30 °C. Bacteriorhodopsin was isolated by other standard methods reported in literature.	0.16	[53, 168]
Xanthophylls carotenoids (yellow)	Bacteria isolation was carried out by suspending collected soil containing biomaterials in distilled water. Samples were stirred vigorously, incubated at 28 °C for 1 h, and seeded on R2A agar plates for two days. The	0.0323	[56, 169, 170]

Table 3 (*continued*)

Bacterial Pigment	Remarks on Bacteria Isolation and Pigment Extraction	η (%)	Ref.
	streak plate method was used to obtain pure cultures where selected isolates were identified by 16S rRNA sequencing. Pigments were extracted using DNeasy® Blood & Tissue Kit (Qiagen) with the amplification steps including initial denaturation final extension.		
Xanthophylls carotenoids (red)	Pigment Extraction as xanthophylls carotenoids (yellow).	0.0332	[56, 169, 170]
Xanthophylls carotenoids (PURE orange)	Xanthophylls pigments were extracted from cells grown in R2 medium, centrifuged to discard the uncolored supernatants while suspending pellet and slime phases in 98% ethanol, and then heated at 60 °C for 1 h until reddish pigments turned to orange. Samples were then centrifuged again, and supernatants were filtered with sterile membrane. Extracted carotenoids from hymenobacter sp. were kept at −20 °C in darkness for future use.	0.008	[81]
Xanthophylls carotenoids (RAW orange)	Pigment Extraction as xanthophylls carotenoids (PURE orange).	0.03	[81]
Xanthophylls carotenoids (Cocktail)	Pigment Extraction as xanthophylls carotenoids (PURE orange).	0.009	[81]
Lycopene carotenoids	No isolation was there, instead cloning of bacterial strains was carried out within E. coli BL21 cells to synthesize and overproduce the photoactive pigment lycopene.	0.057	[82]
RC photosystem I trimer (PSI)	Trimeric PSI was isolated from the thylakoids of the thermophilic cyanobacteria thermosynechococcus elongates. PSI was isolated from frozen cells, resuspended in wash buffer and sorbitol, adjusted to a specific chlorophyll a content, and then homogenized. Lysozyme was added to the mixture prior incubation for 2 h at 37 °C with shaking. Resultant mixture was centrifuged to discard supernatant; remaining pellet phase was resuspended, passed twice through French Press (Amino) at a cell pressure of 20,000 psi, and washed with 3 M NaBr. Density gradient centrifugation was performed prior to collection of the lowest green bands of pooled PSI samples diluted with dialysis against MES and anion exchange column.	0.08	[83, 171]

Zanjanchi and Beheshtian (2019) identified carotenoids, chlorophylls, and anthocyanins to be the most appropriate dyes for achieving high V_{oc} according to the density functional theory (DFT) calculations [148]. Pandey (2018) reported the earlier attempts of utilizing naturally-sensitized dyes (e.g. chlorophyll, betanins, carotenoids, anthocyanins, and tannins) extracted from flowers, leaves, and roots of plants to be used in DSSCs. A PCE of 2% has been accomplished using a cocktail of natural dyes from possible broadening of light-absorption

Table 4

Theoretical HOMO/LUMO energy levels of different and common biomolecular dyes as reported in literature with their corresponding absorption maximum (bandgaps in eV) required for electron photoexcitation.

Pigment Class and/or TiO$_2$	Biomolecular Dye Name	Energy (eV)[a]		Absorption Maximum (eV)		Ref.
		HOMO	**LUMO**	**Theoretical**	**Experimental**	
Anthocyanin	4′-Hydroxyflavylium	−5.67	−2.90	2.78	3.26	[177]
	3′,4′-Dihydroxyflavylium	−5.49	−2.93	2.60	2.51	[177]
	3′,4′,5′-Trihydroxyflavylium	−5.45	−2.99	2.54	2.62	[177]
	3′,4′,7-Trihydroxyflavylium	−5.39	−2.83	2.64	2.46	[177]
	7,8-Dihydroxy-4′-methoxyflavylium	−5.32	−2.78	2.13	2.56	[177]
	7,8-Dihydroxy-4-methylflavylium	−5.34	−2.89	2.00	2.33	[177]
	7-Diethylamino-3′,4′-dihydroxyflavylium	−5.07	−2.56	2.56	2.18	[177]
Carotenoid	Bixin	−6.36	−2.09	4.22	–	[178]
	Norbixin	−6.72	−1.71	4.20	–	[178]
	Transbixin	−6.37	−2.14	4.25	–	[178]
	Trans-carotene: B3LYP	−4.40	−2.20	2.20	–	[179]
	13-cis-carotene: B3LYP	−4.40	−2.10	2.30	–	[179]
	9-cis-carotene: B3LYP	−4.40	−2.10	2.30	–	[179]
	Phytofluene: B3LYP	−4.70	−1.50	3.20	–	[179]
	Zeaxanthin: B3LYP	−4.40	−2.20	2.20	–	[179]
	Trans-carotene: AM1	−7.60	−0.90	6.70	–	[179]
	13-cis-carotene: AM1	−7.60	−0.90	6.70	–	[179]
	9-cis-carotene: AM1	−7.60	−0.90	6.70	–	[179]
	Phytofluene: AM1	−7.90	−0.60	7.30	–	[179]
	Zeaxanthin: AM1	−7.70	−1.00	6.70	–	[179]
	Trans-carotene: PM3	−7.80	−1.10	6.70	–	[179]
	13-cis-carotene: PM3	−7.80	−1.10	6.70	–	[179]
	9-cis-carotene: PM3	−7.80	−1.10	6.70	–	[179]
	Phytofluene: PM3	−8.00	−0.70	7.30	–	[179]
	Zeaxanthin: PM3	−7.80	−1.10	6.70	–	[179]
	Trans-carotene: ZINDO/S	−6.30	−1.10	5.20	–	[179]
	13-cis-carotene: ZINDO/S	−6.40	−1.20	5.20	–	[179]
	9-cis-carotene: ZINDO/S	−6.40	−1.00	5.40	–	[179]
	Phytofluene: ZINDO/S	−6.70	−0.50	6.20	–	[179]
	Zeaxanthin: ZINDO/S	−6.30	−1.10	5.20	–	[179]
Chlorophyll	Chlorin e$_6$ derivative 4	−6.07	−1.94	4.13	1.82	[180]
	Chlorin e$_6$ derivative 6	−6.07	−1.93	4.14	1.82	[180]
	Chlorin e$_6$ derivative 7	−6.07	−1.93	4.14	1.82	[180]
Cyanine	CyA	−5.40	−3.90	1.50	–	[181]
	CyBI (long alkyl chains)	−5.20	−4.20	1.00	–	[181]
	CyBs (short alkyl chains)	−5.20	−4.20	1.00	–	[181]
	Heptamethinecyanine dyes (Dye 1)	−4.92	−3.77	1.14	1.50	[176]
	Heptamethinecyanine dyes (Dye 2)	−4.88	−3.85	1.02	2.20	[176]
Xanthene[b]	mp-SFX-3PA	−5.08	−2.25	2.83	–	[182]
	mm-SFX-3PA	−5.08	−2.27	2.81	–	[182]
	mp-SFX-2PA	−4.92	−1.98	2.94	–	[182]
	mm-SFX-2PA	−4.89	−1.97	2.92	–	[182]
	Spiro-OMeTAD	−4.83	−1.91	2.92	–	[182]
	MOAF-SFX	−6.02	−2.09	3.93	–	[183]
	DMOAF-SFX	−5.93	−2.01	3.92	–	[183]
	MAF-SFX	−6.08	−2.14	3.94	–	[183]
	DMAF-SFX	−6.07	−2.14	3.92	–	[183]
	FAF-SFX	−6.10	−2.14	3.95	–	[183]
	PFX[c]	−5.50	−2.58	2.92	–	[184]
	PTXT[c]	−5.28	−3.05	2.23	–	[184]
	PEXE[c]	−4.48	−2.74	1.74	–	[184]
Coumarin dyes	C343,	−3.22	−1.03	2.19	–	[185]
	NKX-2311	−1.88	−0.41	1.47	–	[185]
	NKX-2586	−1.66	−0.34	1.31	–	[185]
	NKX-2753	−1.75	−0.43	1.31	–	[185]
	NKX-2593	−1.72	−0.46	1.25	–	[185]
	NKX-2311	−5.33	−2.74	2.59	2.46	[186]
	NKX-2311-DP[d]	−4.97	−2.04	2.93	2.74	[186]
	NKX-2593	−5.11	−2.84	2.27	2.08	[186]
	NKX-2593-DP[d]	−4.87	−2.18	2.69	2.44	[186]
TiO$_2$	–	−7.46	−3.28	4.18	3.49	[186]

[a] HOMO/LUMO energies determined from theoretical time dependent and density functional theory (TD-DFT) studies as reported in referenced literature.

[b] Xanthene in Spiro[fluorene-9,9′-xanthene] hole transporting materials (SFX-based HTM) is used in perovskites solar cells.

[c] Fluorene-xanthene-based hybrid polymer in 0.1 M TBAPF6/CAN.

[d] NKX-2311-DP and NKX-2593-DP are deprotonated dyes.

spectrum [149]. Iqbal et al. (2019) summarized the use of different plant-based biomolecular dyes for comparisons; chlorophyll from shiso leaves coated over TiO$_2$ and consequent p-CuI deposition showed a maximum PCE of 1.3% [150] and 6.7% (from chlorin e6 derivative 6); pomegranate pigments showed PCE of 2% [151]; and A. amentacea +

P. pterocarpum in water and/or ethanol showed PCE of 7.38 and/or 8.22%, respectively, as reported in Ref. [152] and summarized by Ref. [153]. Calogero et al. (2015) discussed the use of vegetable-based dyes (betalains, carotenoids and chlorophylls) in bio-sensitized DSSCs which showed a maximum efficiency of 2.06% using betalains from wild

sicilian prickly pear (2012) [139] and 0.37% for carotenoids from annatto (2010) [154] and 4.6% using chlorophylls from wakame (2007) [155] under 1 sun irradiation as concluded in Ref. [156].

To critically analyze the above reported results, the authors compared PCEs and J_{sc} (for bio-sensitized DSSCs) when using the uniquely studied protein complexes and carotenoids (extracted from bacterial sources) with the other reported DSSCs PCEs using biomolecular photosensitizers extracted from plants, flowers, roots, vegetables, leaves, and other conventional biological sources. Fig. 5(A) and Fig. 5(B) show cell performance and attributed bio-pigment sensitization information, respectively. As a rule, highly conjugated structures (n > 13) with many anchoring groups are desired to develop visible-NIR absorption and electron injection, respectively, improving the cell performance [107–109]. Evidently, this is only an approximation to attribute the biomolecular structure to dye photosensitization ability, knowing that many other unknown parameters and bio details should be analyzed in future studies. This might explain the reasons behind the low PCEs (for the same pigment classes) of bacterial-based pigments, Fig. 5(A), as compared to their plant-based biological pigment counterparts, Fig. 5(C).

The state-of-the-art in solid-state mediators show their promising emergence to be utilized in metal-based or naturally-sensitized DSSCs. Solid-state DSSCs suffer from inadequate nanopore filling, low conductivity, and crystallization of hole-transport materials (HTMs) [157]. However, Cao et al. (2017) [157] reported a highly efficient (11%) stable solid-state TiO$_2$-based DSSCs using metal sensitizer (Y123) with the amorphous Cu(II/I) as a HTM conducting holes by rapid hopping [157]. The combination of metal-free natural-based dyes with solid-state redox mediators have been also investigated in various studies [158–162]. Natural dyes extracted from amaranthus caudatus flowers were tested against a polymer gel electrolyte [2-methylImmidazolium iodide (EMIM-I) + sodium iodide (BDH)] in a TiO$_2$ DSSC showing a PCE of 0.61% (with FF >50%, and IPCE 4.7%–5.2%) [158]. Bella et al. (2017) [159] investigated the utilization of (TiO$_2$/cellulose)-photoanodes and cellulose as a paper-based quasi-solid state electrolyte for bio-sensitized DSSCs. The bio-derived paper-based electrolyte/electrode achieved high PCEs of 3.55–5.20% with 96% sustainable efficiency retention for up to 1000 h (under AM1.5). [159]. Rapsomanikis et al. (2016) [160] extracted red seaweed (red algae) pigments to be used as a natural sensitizer in a prefabricated quasi-solid state TiO$_2$ DSSCs, which showed J_{sc} of 1.26 mA cm^{-2} and V_{oc} of 0.66 V. Suzuka et al. (2016) [161] designed a highly reactive nitroxide redox quasi-solid DSSCs molecularly integrated with indoline organic dyes. Long alkyl chains present in the indoline structure enhance dye interactions with the radical mediator suppressing possible interfacial recombination and facilitating charge transport. The fabricated cell achieved a conversion efficiency of 10.1% under 1-sun illumination [161]. Indolines (C$_8$H$_9$N) can be synthesized from reduction of indoles (C$_8$H$_7$N) with sodium cyanoborohydride in carboxylic acids as reported by Kumar (1983) [163], where indoles can be extracted from some flower oils (jasmine), coal tar, and some bacteria [164]. Yazie et al. (2016) [162] constructed a quasi-solid state bio-sensitized DSSC [FTO/TiO$_2$/dye/quasi-solid-electrolyte/PEDOT/FTO] using bougainvillea spectabilis pigments which achieved a PCE of 0.175% with absorbance 395–750 nm [162].

5. Bacteria isolation and extraction processes of bimolecular pigments

Biomolecular pigments can be extracted from various biomaterials including: (i) plant extracts: fruits, flowers, leaves, seeds, peels, and vegetables, (ii) different amino acids and proteins, and (iii) nucleic acids DNA, fungi, and bacteria (bacteria proteins/carotenoids our focus in this work!). The extracted biomolecules (natural products) may also be used as raw materials for cost-effective and green synthesis of carbon quantum dots (C-QDs) or graphene quantum-dots (Q-QDs) utilized for

photoluminescence and optoelectronic applications (e.g. C-QDs and Q-QDs can be used as a counter electrode in DSSCs for efficient electron collection and current generation) [165].

Extraction of natural dyes is a complex process and it requires understanding the nature of the coloring materials and identifying their solubility characteristics. There are several extraction methods which can be used to extract the coloring matter or pigments from natural dye-bearing materials contained in bacteria, plants, and animal constituents. Water-insoluble fibers, carbohydrates, protein, chlorophyll, and tannins are some examples of targeted materials to be extracted for preparing purified natural dyes. The different common methods used for the extraction of coloring materials are: (i) aqueous extraction, (ii) alkali or acid extraction, (iii) microwave and ultrasonic assisted extraction, (iv) fermentation, (v) enzymatic extraction, and (vi) solvent extraction. The aqueous extraction is utilized for extracting dyes from plants by breaking the dye-containing materials, sieving undesired residues, soaking materials in water (overnight), boiling and filtering followed by centrifuging to separate residual matter. Alkali or acid extraction is used for extraction of dyes from flowers as in tesu (buteamonosperma), some flavone dyes (using acidified water) and for dyes having phenolic groups (soluble in alkali); acid hydrolysis occurs from addition of the acid or alkali facilitating the hydrolysis of glycosides in the dyes which can be later precipitated. Microwave and ultrasonic assisted extraction require treatment of dye-containing materials (e.g. plants) in water or any other solvent in the presence of ultrasound; creation/collapse of bubbles increases the extraction efficiency due to applied stress on materials. Fermentation utilizes produced enzymes from the atmosphere/surrounding materials as in harvesting indigo leaves soaked in water for about 10–15 h (glucosideindican breaks down into glucose and yellowish indoxyl by the indimulsin enzyme). Enzymatic extraction uses enzymes including cellulase, amylase, and pectinase for the extraction of dyes from complex plant tissues containing cellulose, starches, and pectins as binding materials. Solvent extraction requires organic solvents (e.g. acetone, chloroform, ethanol, and methanol) or water/alcohol mixtures to extract water-soluble and alcohol-soluble substances from plants which are then purified [166]. Table 3 shows isolation and extraction processes used for separating bacteria and obtaining bacterial-based biomolecular pigments in the various reviewed studies on bio-sensitized DSSCs.

6. Bandgap energies of biomolecular dyes

In biomolecular organic dyes, two typical energy levels exist for electrons called LUMO and HOMO levels. Under illumination, dye molecules get excited allowing electron injection into the CB of the semiconductor as long as LUMO energy level is closer to the vacuum level and higher than semiconductor CB. Effective electron-diffusion and high dye reduction rates occur with the existence of large energy difference between dye-HOMO and electrolyte-redox-potential [139]. Dye light-absorption abilities depend exclusively on HOMO/LUMO energy potential levels and other unknown parameters. HOMO/LUMO molecular orbitals and electron distribution within the dye [172,173] can be utilized to predict quantum chemistry and electron transport to/from the D–π–A dye conjugated structures [174,175]. Electrochemistry calculations show that dye reduction and oxidation potentials occur at the excited state (LUMO) and the ground state (HOMO), respectively. Determination of redox potential can be attributed to the dye bandgap calculated from electrochemical methods and/or UV–Vis absorbance (Tauc plots). Electron delocalization occur with minimum absorbed photon energy yielding in the excitation of the ground state populations (HOMO), delivering electrons to the LUMO moieties through biomolecular conjugated-bridges [176]. Bandgap energies can be calculated from the difference between HOMO to LUMO levels ($E_g = E_{LUMO} - E_{HOMO}$), that is typically desired to be lower than the semiconductor bandgap (e.g. TiO$_2$ or ZnO; <3.2 eV). For example, for cyanine dyes HOMO (−5.73 eV) and LUMO (−3.82 eV) at 590 nm which is equivalent

to a molecular cyanine bandgap of 1.91 eV [144]. Table 4 shows the theoretical HOMO/LUMO energy levels for different biomolecular dyes and their corresponding bandgaps (eV) required for electron photoexcitation.

Theoretical-average HOMO-to-LUMO bandgaps of 2.46, 5.22, 4.13, 1.13, 3.15, and 2.22 eV were calculated from Table 4 for anthocyanin, carotenoid, chlorophyll, cyanine, xanthene, and coumarin, respectively. Correlating the determined biomolecular bandgap energies with the dye contribution in bio-sensitized DSSC performance of anthocyanin 1.67–3.27% [140], carotenoid 0.58% [140], chlorophyll 4.6% [155], cyanine dyes 4.8–7.62% [143,144], xanthenes 1.56% [145], coumarin dyes 7.7–9% [146,147] lead to understand the role of HOMO/LUMO in explaining dye absorption abilities. It is more probable that low dye bandgaps result in enhanced HOMO-electron excitation and e-h pair generation. This is clear from our valid comparison where anthocyanin, cyanine, and coumarin dyes showed the highest bio-sensitized DSSC efficiency >3.27% and up to 9% due to their low bandgaps <2.46 eV. On the contrary, both carotenoid and xanthenes dyes showed very low cell performance <1.56% due to their high bandgaps >3.15 eV. However, the bandgap is not the only parameter controlling the dye absorbance rate, since an exception was noticed with chlorophyll dyes where high performance is observed with high bandgaps which may be explained by the 'relative state of HOMO-level vs. SHE and its correspondence to the CB-level vs. SHE' or by other unknown phenomena such as impact of existing functional groups, dye/semiconductor interactions, and bonding mechanisms changing the photosensitization performance.

Relating the found bandgaps with the studied absorption performance of biological dyes utilized in bio-sensitized DSSC systems is important to critically analyze bandgap association with photosensitization. From Table 4, bio-sensitized DSSC performance using various biomolecular dyes were found as the following: chlorophyll a (PPB) + carotenoids (Spx) 4%, carotenoids 0.009–0.057% (from chromatophores, xanthophylls, or lycopene), and proteins 0.08–0.57% (from LH2, RC, LHII, BRs, PSI). Since proteins and carotenoids are two interrelated biological complexes, they showed similar photosensitization behavior with bio-sensitized DSSC performance within the same boundary limits reported in the literature. Combined dyes (e.g. chlorophyll/carotenoids) can enhance the bio-DSSC performance up to 4% attributed to the low bandgap of chlorophyll <4.13 eV, where the authors believe that high efficiency can be approached using low-bandgap cyanine and coumarin dyes. The requirement for 4.18 eV theoretical bandgap energy for TiO_2 (Table 4) is apparent; however, with the use of bio-dyes, it is possible to excite electrons to a more positive LUMO level for easy electron injection into the semiconductor CB enhancing charge carriers separation and current generation.

7. Challenges and developments in DSSCs

7.1. Photoanode degradation

Excessive ultraviolet (UV) radiations and oxygen environments cause quick dye degradation of the pigmented-photoanode in DSSCs. Hence, it is important to apply a protective layer such as a UV protection foil and/or UV absorbing luminescent chromophores on top of the photoanode for the protection of the pigmented-layer from high UV radiations. Moreover, the addition of antioxidants to the applied pigments might be useful in protecting the pigmented-photoanode from oxidation and further degradation [52].

7.2. Stability of liquid-based DSSCs and thermal stresses

Changing the conventional DSSC liquid electrolyte with a solid-state gel electrolyte would enhance system stability. Liquid electrolytes pose a major design downside in DSSCs because they require an appropriate encapsulation to prevent leakage and contamination which, if not prevented, would lead to stability and high-temperature operations issues.

Liquid expansion occurs in high-temperature environments resulting in high stresses and disruption of electrons transport [187]. To overcome stability issues, a solid-state gel electrolyte is suggested to improve device stability, facilitate electron transfer, and increase the conversion efficiency of DSSCs as previously verified in a solid-state mesoscopic-perovskite-DSSC with >15% efficiency [11,188,189]. Replacement of the traditional iodide/triiodide redox electrolyte with cobalt complexes is another alternative for achieving better cell performance and stability [40,46]. Gratzel et al. [84] showed a DSSC with PCE of 10.3% from combining metal-free (DHO-TPA)-Dye 1 "phenyldihexyloxy-substituted TPA" with a cobalt redox electrolyte which optimized dye conjugated bridge.

High-temperature environments negatively impact DSSCs performance and long-term stability because of electrolyte evaporation and permeation of water or oxygen molecules disrupting redox reactions and dye regeneration [190–192]. Liquid-iodide-based DSSCs show limited performance in the outdoor applications in high-temperature regions because of the low electrolyte boiling points (highly volatile) [192]. Solid-state electrolytes maintain cell performance over long periods where the normalized efficiency previously observed to only decrease from 1 to 0.85 over 40 days operation period for solid-state systems using PMMA-EC/PC/DMC-NaI/I_2 as compared to a decrease of 1 to 0.3 in liquid-based systems [193]. Kim et al. (2015) [194] noted that charge recombination rates will increase from reductions in liquid viscosities at high temperatures; with increasing temperatures from −4 to 60 °C, the DSSC [TiO_2/Ru (N719) dye/Iodide-electrolyte/Pt] PCE decreased from 7.25 to 5.67% (due to the lower observed V_{oc} and the reduced J_{sc} and electron lifetime) [194]. Bari et al. (2011) [195] reported that thermal stresses (60–85 °C) can drastically decrease J_{sc} (3-fold decrease over 115 h) reducing the efficiency of conventional Ru-dye TiO_2 iodide-based DSSCs, due to hindered dye photo-absorption capabilities and degraded TiO_2/Ru-dye/electrolyte interface. On the contrary, Berginc (2008) [196] concluded that a slight increase in temperatures (<40 °C) may enhance J_{sc} due to the developed diffusion of tri-iodide, but further temperature increase would facilitate recombinations especially at low iodide concentrations (<0.05 M I_2) [196]. High temperatures may also promote recombination of generated electrons with electrolyte species due to shifting in the semiconductor CB [197–199]. Thermal stresses change energy levels where electron trapping occurs from upward shifting of the Fermi level (E_F) towards the CB edge (E_{CB}) knowing that the activation energy (E_a) of recombination is proportional to ($E_{CB}-E_F$) [200,201]. However, upward shifting of E_F is reported to promote V_{oc} in doped photoanodes [202,203] and bromide perovskites [204] which is explained by the increased electron concentration and partially filled surface traps [205]. Despite that, V_{oc} monotonically decreases at high temperatures due to trapped electrons leading to a lower conversion efficiency [196,206]. Under AM1.5 illumination, M. Grätzel was capable to design a DSSC surviving a high temperature of 80 °C for 1000 h and showed a stable photovoltaic performance up to 60 °C [207].

Caffeine (1,3,7-trimethylxanthine) containing two conjugated carboxyl groups can hinder thermal stability issues and improve cell electronic properties as observed when incorporated in perovskite cells (CsFAMAPbI$_3$ active layers) maintaining 19.8% efficiency at 85 °C [208–210]. Caffeinated films extended electron lifetime from 51.9 to 114.3 ns demonstrating lower trap density and passivated defects to avoid recombination [208]. Stability of caffeine-incorporated perovskites (MAPbI$_3$) films is enhanced from suppression of ion migration (Pb^{2+}) due to restrained Pb–I stretching vibrations result from the increased activation energy (from C=O bonds) and delocalized electrons (from conjugation with C=C bonds) [211,212]. The authors believe that caffeine can also be applied in DSSCs with optimal added ratio from 1 to 2 wt. % for superior thermal stability (<100 °C) with lower hysteresis index preserving the cell efficiency [208,211,212].

7.3. Low cell efficiency

In the context of nanomaterials, nano-dispersed copper (Cu) embedded in an inert carbon and dispersed on TiO_2 photoelectrode films has been claimed to increase the DSSC overall efficiency by 23% as compared to pure TiO_2 electrodes [213]. Engineered *E. coli* cells (producing lycopene carotenoids) coated with TiO_2 nanoparticles have been used as a photoanode in DSSCs due to the absence of any reduction-oxidation reactions in the operational range of −0.1 to 0.2 V suggesting that there is: (i) a much lower back electron transport, (ii) a reduced electron recombination with the oxidized dye and/or oxidized redox electrolyte, and (iii) a fairly stable pigmented electrode for bio-photovoltaic applications [82].

7.4. Bio-sensitized DSSCs complications

Chemical processing and coating of biological dyes such as proteins and carotenoids onto semiconductors is not an easy task. A lot of complications and disadvantages arise from scaling of such bio-sensitized DSSCs device which may exhibit low stability and poor long-term performance [214]. Thus, adopting a new design strategy to fabricate such a bilayer dye photoanode structure in an aqueous p-type bio-sensitized DSSCs should be considered for better stability and lower recombination [215].

7.5. Recombination and electron lifetime

Principally, the phase contacts in the compact semiconductor layer (e.g. ITO, TiO_2, and electrolyte) as: (i) TiO_2/electrolyte, (ii) TiO_2/dye, and (iii) ITO/electrolyte interfaces, as shown in Fig. 2(A) and Fig. 2(E), play a crucial role in electron transport influencing recombination dynamics [85,87,96,97]. Here, we are mainly interested in discussing recombination with respect to the dye at either TiO_2/dye or TiO_2/electrolyte (i.e. dye/electrolyte since dye is part of the photoanode) interfaces. Recombination of dye molecules excited electrons arise from two simultaneous competing reactions: (i) recombination with the oxidized dye, and (ii) recombination with the oxidized redox species in the electrolyte [59]. Blocking back electron transport in the semiconductor is critical for lowering recombination rates. TiO_2 is found to be an optimal semiconductor film because it can prevent back electron transport as well as provide a huge surface and contact area to enhance electron injection and electron forward transfer at the TiO_2/dye and TiO_2/ITO interfaces, respectively ,Fig. 2(E), [87,95]. Passivation of recombination centers with 4-tertbutylpyridine can also suppress back electron transport and recombination with oxidized tri-iodide in DSSCs [216]. Furthermore, efficient hindrance of back electron transport to the redox mediator have been achieved through the use of organic sensitizers with long chain alkoxy groups which prevent electrolyte direct contact with TiO_2 surface and increase electron lifetime [217].

7.6. Recombination with the oxidized dye

This recombination occurs due to the electron-transfer across the semiconductor/dye interface ,Fig. 2(E), in the presence of light (does not occur in the dark); denoted as (e1) in Fig. 2(A). Electron coupling between LUMO (excited-state dye orbitals) in dye molecules and the semiconductor CB level ensures the ultrafast electron injection rates. Undesired recombination rates with the oxidized dye are usually low due to the presumed weak electron coupling between HOMO and semiconductor CB levels. This is because most of the oxidized dye molecules are usually regenerated successfully within a short time of 10 ms to 1 s in the presence of a redox electrolyte [59]. However, recombination rates and electron losses are not always low, but they change with the applied driving force (e.g. excited state potential) [218], electron travel distance (semiconductor thickness) [219,220], electron concentration in the semiconductor [221,222], dye structure, dye

orientation on the semiconductor surface, electronic coupling/decoupling properties onto the semiconductor, and available dye anchoring groups and/or linkers [59]. Recombination and regeneration are two dominant competitive processes arise from the oxidized dye in the presence of the redox electrolyte. Fast recombination has been observed by Wiberg et al. [223] through a femto-second laser characterization on the L2 and L2A3 dyes with different surface anchoring groups where fast recombination occurred because electrons were injected into states closer to the semiconductor surface.

7.7. Recombination with the oxidized redox electrolyte species (acceptor)

DSSCs with efficient dye regeneration mostly suffer from electron losses due to recombination with the redox electrolyte at the dye/electrolyte interface ,Fig. 2(E), and denoted as (e2) in Fig. 2(A). This is possibly from dominant intermolecular interactions which are more prominent in oxidized-redox recombination. In liquid-state DSSCs, degree of recombination with the oxidized electrolyte is restrained by a 10:1 iodide-to-iodine concentration ratio (e.g. 500:50 mM) owing to the efficient mass transportation provided by iodide and efficient reduction of iodine ions at the cathode side. The combination of (iodine/triiodide) with small amounts of acceptor species is important for achieving high photocurrents from hindered recombination rates with the electrolyte (dark current) [59]. Electron lifetime (spent time of excited electrons after e-h generation and before recombination) varies with dye structure and the iodine concentration; a decrease in electron lifetime for a TiO_2-based DSSC from around 5–10 s to 0.1 s was observed for L0 dye with an increase in both iodine [I_2] concentration (at V_{oc} = 0.5 V) and applied voltage from 0.2 to 0.7 V. Dye amounts can also impact the electron lifetime where the increase in the organic dye loads result in longer electron lifetimes and enhanced photocurrents. Long minority carrier lifetimes indicate a higher V_{oc}; hence, resulting in a more efficient DSSC [59]. Previous conclusions have been only proved for ruthenium-based DSSCs. However, the use of organic dyes with extended linker conjugation improve dye absorption properties but, at the same time, linkers may introduce more recombination sites for the redox electrolyte lowering V_{oc} [59,224]. This might be attributed to the large organic dye molecules and electrostatic interactions at the dye/electrolyte interface [224]. To date, organic pigments show excellent photocurrents with low V_{oc} values due to excess interfacial electron recombination as compared to ruthenium-based dyes [224,225]. Oxidized redox recombination is totally dependent on the dye structure where dense dye layers, large molecules, and/or alkyl chain linkers are not preferred due to their prominent effect on shortening electron lifetime and progressing recombination [59,224,226–228]. The use of insulating layers (e.g. SiO_2, Al_2O_3, and ZrO_2) on TiO_2 films have been proposed to mitigate interfacial recombination dynamics since excess metal oxides will act as a physical barrier for back electron transport to the electrolyte, but with decreased probability for the desired electron injection [85,229].

7.8. Counter electrode stability and scalability

Counter electrodes (CEs) in DSSCs have a critical role in determining the cell efficiency depending on their abilities to collect electrons coming for the photoanode side. A number of parameters should exist for the selection of optimal and scalable CEs: (i) sheet resistance, (ii) catalytic activity, (iii) chemical stability, and (iv) cost [49,190,230–234]. For an optimized cell, sheet resistance must be as low as possible (for effective electron transport), catalytic activity should be very high to reduce redox species in liquid solar cells or to collect holes in solid-state DSSCs for redox regeneration, CE materials must possess a noble-like behavior as in Pt electrodes for corrosion stability, and lastly the cost should be reasonable such as using carbon-based materials for possible scalability. Pt deposited on TCO glass sheets have been conventionally used as the standard CE for DSSCs to get the best

performance due to its high catalytic activity, excellent conductivity, and corrosion stability in liquid-based systems [235–238]. However, Pt is highly expensive for large-scale applications due to its scarcity; the development in Pt-free CEs should be pursued to have cost-effective and scalable CEs [230].

Recently, Wang et al. (2012) [230] utilized graphene-based composites for CEs in DSSCs owing to graphene excellent conductivity and high electrocatalytic activity. Carbon-based CEs showed high photo-conversion of 6.67, 3.9, 4.5, and 7.7% for CEs from graphite [239], activated carbon [240], single-walled carbon nanotubes (SWCNTs) [241], and multi-walled carbon nanotubes (MWCNTs) [242], respectively [230]. Graphene-composite CEs achieved efficiencies up to 2.5, 7.6, 7.5, 5.7, 8.5, 7.8, and 9.8% for cotton-based graphene, graphene/Pt, graphene/MWCNTs, $Ni_{12}P_5$/graphene, graphene-NiS_2, 3D honeycomb-like structured graphene (HSG), and 2D-graphene/3D-graphene-oxide, respectively [230,232,243–252]. Ye et al. (2015) [253] reported on using Pt-free materials and inorganic compounds (e.g. CoS_2, $CuInS_2$, Cu_2ZnSnS_4, Co_9S_8, Sb_2S_3, Cu_2S, and $CoMoS_4$) [254–259], carbides (e.g. TiC) [260], nitrides (e.g. TiN and ZrN) [261,262], phosphides (e.g. Ni_2P and Ni_5P_4) [263], tellurides (e.g. CoTe and $NiTe_2$) [264], conductive polymers (e.g. PANI, PEDOT, and PPy) [265–270] as cost-effective, highly conductive, transparent, and stable CEs for DSSCs.

8. Conclusions and outlook

We demonstrated the potential of using bacterial-based biomolecular pigments extracted from protein and carotenoid complexes. Bacterial-pigments are found to be promising photosensitizer candidates since they are cost-effective, scalable, renewable, sustainable, environmental-friendly, biodegradable, and noncarcinogenic. Biomolecular pigments can be extracted from plant extracts, amino acids, and bacteria. The authors have elucidated the structural components of DSSCs (anode, photosensitizer, electrolyte, and counter electrode) with elaborated discussions on the DSSCs working mechanism and recombination kinetics. Performance parameters including J_{sc}, V_{oc}, FF, and PCE are strongly associated with the dye light-absorption capabilities for the injection of photoexcited electrons. Current knowledge and recent advancements on novel biological pigments in DSSCs were reviewed and discussed with emphasis on: (i) bio-dyes bacterial sources, (ii) pigments chemical structure and bio-information (e.g. anchoring groups and conjugation), (iii) bacteria isolation for pigment extraction, (iv) dye bandgaps, and (v) photoelectrochemical performance of bio-sensitized DSSCs using biological dyes for solar-to-electricity conversion. Discussed bacterial-based pigments were RC proteins, BChl, chromato-phores, LH2, LH4, RC PPCs, LHCII, BR proteins, xanthophylls carotenoids, lycopene carotenoids, and RC PSI.

Chromatophores integrated with bio-electrolyte provide a unidirectional flow of electrons from good components coupling. Both DSSCs PCE and J_{sc} linearly increase with the number of conjugated π-bonds that exist in the bio-dye. As a rule, highly conjugated structures (n > 13) with many anchoring groups develop pigment visible-NIR absorption and electron injection. Pigments with many carboxyl/hydroxyl groups show enhanced dye/semiconductor attachment and lower charge resistance. RC-sensitized DSSCs have better photoelectric properties than LH2 due to its greater charge separation. The combination of pigments (hybrid or cocktail dyes; e.g. chlorophyll/carotenoids achieved 4% PCE) boosts sensitizer photosensitivity and broadens bio-pigment absorbance. Some of the strategies to overcome UV/high-temperature degradation of the photoanode and/or bio-pigment monolayer include: (i) antioxidants protect bio-dye molecules from excess UV radiations, (ii) solid-state gel redox improve device stability, dye neutralization, and maintain performance over long periods, and (iii) bilayer dye photoanode structure hinders dye degradation and lowers recombination. Furthermore, insulating layers and passivation of recombination centers suppress back electron transport, keeping in mind that electron lifetime changes with iodine concentration, applied

voltage, and dye amounts.

Protein complexes (LH2, BR, RC) and chlorophyll a derivatives combined with carotenoids were the most promising bacterial-based sensitizers achieving DSSCs PCE of 0.16–0.57% and 4%, respectively. Xanthophylls carotenoids (from Antarctic bacteria) showed the lowest bio-sensitized DSSCs performance of 0.008–0.03%, where poly-saccharides co-adsorbents improve xanthophylls bonding/anchoring onto TiO_2 nanoparticles for enhanced charge carriers transport. Theoretical-average HOMO-to-LUMO bandgaps of 2.46, 5.22, 4.13, 1.13, 3.15, and 2.22 eV were calculated for anthocyanin, carotenoid, chlorophyll, cyanine, xanthene, and coumarin, respectively. Low dye bandgaps (<2.46 eV) are expected to enhance HOMO-electron excitation and PCE as in coumarin. To date, optimization of photosensitizers of either expensive/harmful conventional metal-based pigments (e.g. N3, N719, and N749 Ru-dyes) or common plant-based pigments extracted from flowers, leaves, and fruits (e.g. anthocyanins, flavonoids, carotenoids) have shown a maximum DSSCs PCE of 10.3–13% and 0.05–1.7%, respectively. The high conversion of metal-based DSSCs is comparable to the maximum PCE observed in TiO_2-based DSSCs using plant-based coumarin dyes (9%) or from [A. amentacea + P. pterocarpum] pigments (8.22%). Nitroxide redox quasi-solid DSSCs integrated with long alkyl chains indoline organic dyes showed PCE of 10.1% due to enhanced dye/redox interactions and suppressed recombination. Photosensitizers initiate electron injection that is the most critical first step for charge transfer. Fabricating a bio-sensitized DSSC with an ideal environmental-friendly bio-pigment can drastically boost-up photo-generated excitons for having a significant gain in DSSC solar-to-electricity conversion efficiency.

This review tackled current technological advancements in biomolecular photosensitizers for various bio-photoelectronic, photovoltaic and optoelectronic passive-organisms applications; to catch up with the current progress in bio-photosensitization for DSSCs and bridge the gap between science and applications in this emerging area. We anticipate that this review will motivate photovoltaic researchers towards integrating biomolecular photosensitizers and bio-modified photosensitized anodes in many photovoltaic and optoelectronic applications such as: (i) DSSCs and multi-junction photovoltaic cells for solar-to-electricity applications, (ii) photodiodes and phototransistors for current regulations and signal switching, (iii) photodetectors for gas, thermal and catalytical sensing, (iv) piezoelectrics for charge accumulation and response to various mechanical stresses, (v) flexible electronics for printed bio-pigmented silver circuit films and solar-pigmented clothing, (vi) bio-light-emitting diodes (bio-LEDs) for light generation from packaging luminescent proteins, and (vii) photo-tunneling junctions and quantum electronics for efficient light harvesting, electron excitation, and solar energy utilization.

Conflicts of interest

There are no conflicts of interest to declare.

Acknowledgements

References

[1] Shafiee S, Topal E. When will fossil fuel reserves be diminished? Energy Policy 2009. https://doi.org/10.1016/j.enpol.2008.08.016.

[2] Parida B, Iniyan S, Goic R. A review of solar photovoltaic technologies. Renew Sustain Energy Rev 2011. https://doi.org/10.1016/j.rser.2010.11.032.

[3] Pi X, Zhang L, Yang D. Enhancing the efficiency of multicrystalline silicon solar cells by the inkjet printing of silicon-quantum-dot ink. J Phys Chem C 2012. https://doi.org/10.1021/jp307078g.

[4] Dekkers HFW, Carnel L, Beaucarne G. Carrier trap passivation in multicrystalline Si solar cells by hydrogen from SiN$_x$:H layers. Appl Phys Lett 2006. https://doi.org/10.1063/1.2219142.

[5] Lipiński M, Panek P, Witek Z, Beltowska E, Ciach R. Double porous silicon layer on multi-crystalline Si for photovoltaic application. Sol Energy Mater Sol Cells 2002. https://doi.org/10.1016/S0927-0248(01)00174-X.

[6] Klampaftis E, Richards BS. Improvement in multi-crystalline silicon solar cell efficiency via addition of luminescent material to EVA encapsulation layer. Prog Photovolt Res Appl 2011. https://doi.org/10.1002/pip.1019.

[7] Sarti D, Einhaus R. Silicon feedstock for the multi-crystalline photovoltaic industry. Sol Energy Mater Sol Cells 2002. https://doi.org/10.1016/S0927-0248(01)00147-7.

[8] Noel NK, Stranks SD, Abate A, Wehrenfennig C, Guarnera S, Haghighirad AA, et al. Lead-free organic-inorganic tin halide perovskites for photovoltaic applications. Energy Environ Sci 2014. https://doi.org/10.1039/c4ee01076k.

[9] Tzounis L, Stergiopoulos T, Zachariadis A, Gravalidis C, Laskarakis A, Logothetidis S. Perovskite solar cells from small scale spin coating process towards roll-to-roll printing: optical and Morphological studies. Mater. Today Proc. 2017. https://doi.org/10.1016/j.matpr.2017.04.117.

[10] Zhang W, Eperon GE, Snaith HJ. Metal halide perovskites for energy applications. Nat Energy 2016. https://doi.org/10.1038/nenergy.2016.48.

[11] Liu M, Johnston MB, Snaith HJ. Efficient planar heterojunction perovskite solar cells by vapour deposition. Nature 2013. https://doi.org/10.1038/nature12509.

[12] Park NG. Perovskite solar cells: an emerging photovoltaic technology. Mater Today 2015. https://doi.org/10.1016/j.mattod.2014.07.007.

[13] Green MA, Ho-Baillie A, Snaith HJ. The emergence of perovskite solar cells. Nat Photonics 2014. https://doi.org/10.1038/nphoton.2014.134.

[14] Zhou H, Chen Q, Li G, Luo S, Song TB, Duan HS, et al. Interface engineering of highly efficient perovskite solar cells. Science 2014. https://doi.org/10.1126/science.1254050.

[15] Hodes G. Perovskite-based solar cells. Science 2013. https://doi.org/10.1126/science.1245473.

[16] Jung HS, Park NG. Perovskite solar cells: from materials to devices. Small 2015. https://doi.org/10.1002/smll.201402767.

[17] Tao M. Inorganic photovoltaic solar cells: silicon and beyond. Electrochem Soc Interface 2008.

[18] Miles RW, Zoppi G, Forbes I. Inorganic photovoltaic cells. Mater Today 2007. https://doi.org/10.1016/S1369-7021(07)70275-4.

[19] McCandless BE, Sites JR. Cadmium telluride solar cells. Handb. Photovolt. Sci. Eng. 2011. https://doi.org/10.1002/9780470974704.ch14.

[20] Britt J, Ferekides C. Thin-film CdS/CdTe solar cell with 15.8% efficiency. Appl Phys Lett 1993. https://doi.org/10.1063/1.109629.

[21] Wu X. High-efficiency polycrystalline CdTe thin-film solar cells. Sol Energy 2004. https://doi.org/10.1016/j.solener.2004.06.006.

[22] Kaelin M, Rudmann D, Tiwari AN. Low cost processing of CIGS thin film solar cells. Sol Energy 2004. https://doi.org/10.1016/j.solener.2004.08.015.

[23] Wuerz R, Eicke A, Frankenfeld M, Kessler F, Powalla M, Rogin P, et al. CIGS thin-film solar cells on steel substrates. Thin Solid Films 2009. https://doi.org/10.1016/j.tsf.2008.11.016.

[24] Wada T, Hashimoto Y, Nishiwaki S, Satoh T, Hayashi S, Negami T, et al. High-efficiency CIGS solar cells with modified CIGS surface. Sol Energy Mater Sol Cells 2001. https://doi.org/10.1016/S0927-0248(00)00296-8.

[25] Cuce E, Young C-H, Riffat SB. Thermal performance investigation of heat insulation solar glass: a comparative experimental study. Energy Build 2015. https://doi.org/10.1016/j.enbuild.2014.10.063.

[26] Ameri T, Dennler G, Lungenschmied C, Brabec CJ. Organic tandem solar cells: a review. Energy Environ Sci 2009. https://doi.org/10.1039/b817952b.

[27] Albrecht S, Yilmaz S, Dumsch I, Allard S, Scherf U, Beaupré S, et al. Solution processed organic tandem solar cells. Energy Procedia 2011. https://doi.org/10.1016/j.egypro.2012.11.178.

[28] Hadipour A, De Boer B, Blom PWM. Organic tandem and multi-junction solar cells. Adv Funct Mater 2008. https://doi.org/10.1002/adfm.200700517.

[29] Ameri T, Li N, Brabec CJ. Highly efficient organic tandem solar cells: a follow up review. Energy Environ Sci 2013. https://doi.org/10.1039/c3ee40388b.

[30] Riede M, Uhrich C, Widmer J, Timmreck R, Wynands D, Schwartz G, et al. Efficient organic tandem solar cells based on small molecules. Adv Funct Mater 2011. https://doi.org/10.1002/adfm.201002760.

[31] Meng L, Zhang Y, Wan X, Li C, Zhang X, Wang Y, et al. Organic and solution-processed tandem solar cells with 17.3% efficiency. Science 2018. https://doi.org/10.1126/science.aat2612.

[32] Tvrdy K, Kamat PV. Quantum dot solar cells. Compr. Nanosci. Technol. 2010. https://doi.org/10.1016/B978-0-12-374396-1.00129-X.

[33] Taylor RA, Ramasamy K. Colloidal quantum dots solar cells. SPR Nanosci 2017. https://doi.org/10.1039/9781782620358-00142.

[34] Pan Z, Rao H, Mora-Seró I, Bisquert J, Zhong X. Quantum dot-sensitized solar cells. Chem Soc Rev 2018. https://doi.org/10.1039/c8cs00431e.

[35] Kamat PV. Quantum dot solar cells. Semiconductor nanocrystals as light harvesters. J Phys Chem C 2008. https://doi.org/10.1021/jp806791s.

[36] Nozik AJ, Beard MC, Luther JM, Law M, Ellingson RJ, Johnson JC. Semiconductor quantum dots and quantum dot arrays and applications of multiple exciton

generation to third-generation photovoltaic solar cells. Chem Rev 2010. https://doi.org/10.1021/cr900289f.

[37] Ning Z, Gong X, Comin R, Walters G, Fan F, Voznyy O, et al. Quantum-dot-in-perovskite solids. Nature 2015. https://doi.org/10.1038/nature14563.

[38] O'Regan B, Grätzel M. A low-cost, high-efficiency solar cell based on dye-sensitized colloidal TiO$_2$ films. Nature 1991. https://doi.org/10.1038/353737a0.

[39] Koyama Y, Miki T, Wang XF, Nagae H. Dye-sensitized solar cells based on the principles and materials of photosynthesis: mechanisms of suppression and enhancement of photocurrent and conversion efficiency. Int J Mol Sci 2009. https://doi.org/10.3390/ijms10114575.

[40] Hagfeldt A. Brief overview of dye-sensitized solar cells. Ambio 2012. https://doi.org/10.1007/s13280-012-0272-7.

[41] Bessho T, Zakeeruddin SM, Yeh CY, Diau EWG, Gratzel M. Highly efficient mesoscopic dye-sensitized solar cells based on donor-acceptor-substituted porphyrins. Angew Chem Int Ed 2010. https://doi.org/10.1002/anie.201002118.

[42] Hemalatha KV, Karthick SN, Justin Raj C, Hong NY, Kim SK, Kim HJ. Performance of Kerria japonica and Rosa chinensis flower dyes as sensitizers for dye-sensitized solar cells. Spectrochim Acta Part A Mol Biomol Spectrosc 2012. https://doi.org/10.1016/j.saa.2012.05.027.

[43] Ito S, Miura H, Uchida S, Takata M, Sumioka K, Liska P, et al. High-conversion-efficiency organic dye-sensitized solar cells with a novel indoline dye. Chem Commun 2008. https://doi.org/10.1039/b809093a.

[44] Tan B, Toman E, Li Y, Wu Y. Zinc stannate (Zn$_2$SnO$_4$) dye-sensitized solar cells. J Am Chem Soc 2007. https://doi.org/10.1021/ja070804f.

[45] Woronowicz K, Ahmed S, Biradar AA, Biradar AV, Birnie DP, Asefa T, et al. Near-IR absorbing solar cell sensitized with bacterial photosynthetic membranes. Photochem Photobiol 2012. https://doi.org/10.1111/j.1751-1097.2012.01190.x.

[46] Feldt SM, Gibson EA, Gabrielsson E, Sun L, Boschloo G, Hagfeldt A. Design of organic dyes and cobalt polypyridine redox mediators for high-efficiency dye-sensitized solar cells. J Am Chem Soc 2010. https://doi.org/10.1021/ja1088869.

[47] Dette C, Pérez-Osorio M, Kley CS, Punke P, Patrick CE, Jacobson P, et al. TiO$_2$ anatase with a bandgap in the visible region. Nano Lett 2014;14:6533–8. https://doi.org/10.1021/nl503131s.

[48] Kavan L. Electrochemistry and dye-sensitized solar cells. Curr Opin Electrochem 2017. https://doi.org/10.1016/j.coelec.2017.03.008.

[49] Sugathan V, John E, Sudhakar K. Recent improvements in dye sensitized solar cells: a review. Renew Sustain Energy Rev 2015. https://doi.org/10.1016/j.rser.2015.07.076.

[50] Narayan MR. Review: dye sensitized solar cells based on natural photosensitizers. Renew Sustain Energy Rev 2012. https://doi.org/10.1016/j.rser.2011.07.148.

[51] Mathew S, Yella A, Gao P, Humphry-Baker R, Curchod BFE, Ashari-Astani N, et al. Dye-sensitized solar cells with 13% efficiency achieved through the molecular engineering of porphyrin sensitizers. Nat Chem 2014. https://doi.org/10.1038/nchem.1861.

[52] Hug H, Bader M, Mair P, Glatzel T. Biophotovoltaics: natural pigments in dye-sensitized solar cells. Appl Energy 2014. https://doi.org/10.1016/j.apenergy.2013.10.055.

[53] Molaeirad A, Janfaza S, Karimi-Fard A, Mahyad B. Photocurrent generation by adsorption of two main pigments of Halobacterium salinarum on TiO$_2$ nanostructured electrode. Biotechnol Appl Biochem 2015. https://doi.org/10.1002/bab.1244.

[54] Chen CY, Wang M, Li JY, Pootrakulchote N, Alibabaei L, Ngoc-Le CH, et al. Highly efficient light-harvesting ruthenium sensitizer for thin-film dye-sensitized solar cells. ACS Nano 2009. https://doi.org/10.1021/nn900756s.

[55] Wu W, Xu X, Yang H, Hua J, Zhang X, Zhang L, et al. D-π-M-π-A structured platinum acetylide sensitizer for dye-sensitized solar cells. J Mater Chem 2011. https://doi.org/10.1039/c1jm10942a.

[56] Órdenes-Aenishanslins N, Anziani-Ostuni G, Vargas-Reyes M, Alarcón J, Tello A, Pérez-Donoso JM. Pigments from UV-resistant antarctic bacteria as photosensitizers in dye sensitized solar cells. J Photochem Photobiol B Biol 2016. https://doi.org/10.1016/j.jphotobiol.2016.08.004.

[57] McConnell I, Li GH, Brudvig GW. Energy conversion in natural and artificial photosynthesis. Chem Biol 2010. https://doi.org/10.1016/j.chembiol.2010.05.005.

[58] Mishra A, Fischer MK, Bauerle P. Metal-free organic dyes for dye-sensitized solar cells: from structure: property relationships to design rules. Angew Chem Int Ed Engl 2009. https://doi.org/10.1002/anie.200804709.

[59] Marinado T. Photoelectrochemical studies of dye-sensitized solar cells using organic dyes. 2009.

[60] Galoppini E. Linkers for anchoring sensitizers to semiconductor nanoparticles. Coord Chem Rev 2004. https://doi.org/10.1016/j.ccr.2004.03.016.

[61] Richhariya G, Kumar A, Tekasakul P, Gupta B. Natural dyes for dye sensitized solar cell: a review. Renew Sustain Energy Rev 2017. https://doi.org/10.1016/j.rser.2016.11.198.

[62] Kumara NTRN, Lim A, Lim CM, Petra MI, Ekanayake P. Recent progress and utilization of natural pigments in dye sensitized solar cells: a review. Renew Sustain Energy Rev 2017. https://doi.org/10.1016/j.rser.2017.04.075.

[63] Adedokun O, Titilope K, Awodugba AO. Review on natural dye-sensitized solar cells (DSSCs). Int J Eng Technol IJET 2016. https://doi.org/10.19072/ijet.96456.

[64] Sawhney N, Raghav A, Satapathi S. Utilization of naturally occurring dyes as sensitizers in dye sensitized solar cells. IEEE J Photovoltaics 2017. https://doi.org/10.1109/JPHOTOV.2016.2639343.

[65] Mozaffari SA, Saeidi M, Rahmanian R. Photoelectric characterization of fabricated dye-sensitized solar cell using dye extracted from red Siahkooti fruit as natural sensitizer. Spectrochim Acta Part A Mol Biomol Spectrosc 2015. https://doi.org/10.1016/j.saa.2015.02.003.

[66] Ludin NA, Al-Alwani Mahmoud AM, Bakar Mohamad A, Kadhum AAH, Sopian K, Abdul Karim NS. Review on the development of natural dye photosensitizer for dye-sensitized solar cells. Renew Sustain Energy Rev 2014. https://doi.org/10.1016/j.rser.2013.12.001.

[67] Agarkar SA, Kulkarni RR, Dhas VV, Chinchansure AA, Hazra P, Joshi SP, et al. Isobutrin from butea monosperma (flame of the forest): a promising new natural sensitizer belonging to chalcone class. ACS Appl Mater Interfaces 2011. https://doi.org/10.1021/am200341y.

[68] Wang XF, Fujii R, Ito S, Koyama Y, Yamano Y, Ito M, et al. Dye-sensitized solar cells using retinoic acid and carotenoic acids: dependence of performance on the conjugation length and the dye concentration. Chem Phys Lett 2005. https://doi.org/10.1016/j.cplett.2005.09.020.

[69] Stahl W, Sies H. Antioxidant activity of carotenoids. Mol Asp Med 2003. https://doi.org/10.1016/S0098-2997(03)00030-X.

[70] Wang XF, Koyama Y, Nagae H, Yamano Y, Ito M, Wada Y. Photocurrents of solar cells sensitized by aggregate-forming polyenes: enhancement due to suppression of singlet-triplet annihilation by lowering of dye concentration or light intensity. Chem Phys Lett 2006. https://doi.org/10.1016/j.cplett.2006.01.003.

[71] Wang XF, Matsuda A, Koyama Y, Nagae H, Sasaki S ichi, Tamiaki H, et al. Effects of plant carotenoid spacers on the performance of a dye-sensitized solar cell using a chlorophyll derivative: enhancement of photocurrent determined by one electron-oxidation potential of each carotenoid. Chem Phys Lett 2006. https://doi.org/10.1016/j.cplett.2006.04.008.

[72] Grätzel M. Conversion of sunlight to electric power by nanocrystalline dye-sensitized solar cells. J Photochem Photobiol A Chem 2004. https://doi.org/10.1016/j.jphotochem.2004.02.023.

[73] Dai Q, Rabani J. Photosensitization of nanocrystalline TiO2 films by anthocyanin dyes. J Photochem Photobiol A Chem 2002. https://doi.org/10.1016/S1010-6030(02)00073-4.

[74] Jelle BP, Breivik C, Drolsum Røkenes H. Building integrated photovoltaic products: a state-of-the-art review and future research opportunities. Sol Energy Mater Sol Cells 2012. https://doi.org/10.1016/j.solmat.2011.12.016.

[75] Heiniger LP, O'Brien PG, Soheilnia N, Yang Y, Kherani NP, Grätzel M, et al. See-through dye-sensitized solar cells: photonic reflectors for tandem and building integrated photovoltaics. Adv Mater 2013. https://doi.org/10.1002/adma.201302113.

[76] Lu Y, Yuan M, Liu Y, Tu B, Xu C, Liu B, et al. Photoelectric performance of bacteria photosynthetic proteins entrapped on tailored mesoporous WO3-TiO2 films. Langmuir 2005. https://doi.org/10.1021/la0470129.

[77] Wang XF, Xiang J, Wang P, Koyama Y, Yanagida S, Wada Y, et al. Dye-sensitized solar cells using a chlorophyll a derivative as the sensitizer and carotenoids having different conjugation lengths as redox spacers. Chem Phys Lett 2005. https://doi.org/10.1016/j.cplett.2005.04.067.

[78] Fu Q, Zhao C, Yang S, Wu J. The photoelectric performance of dye-sensitized solar cells fabricated by assembling pigment-protein complexes of purple bacteria on nanocrystalline photoelectrode. Mater Lett 2014. https://doi.org/10.1016/j.matlet.2014.05.054.

[79] Yu D, Zhu G, Liu S, Ge B, Huang F. Photocurrent activity of light-harvesting complex II isolated from spinach and its pigments in dye-sensitized TiO2 solar cell. Int J Hydrogen Energy 2013. https://doi.org/10.1016/j.ijhydene.2013.02.114.

[80] Chellamuthu J, Nagaraj P, Chidambaram SG, Sambandam A, Muthupandian A. Enhanced photocurrent generation in bacteriorhodopsin based bio-sensitized solar cells using gel electrolyte. J Photochem Photobiol B Biol 2016. https://doi.org/10.1016/j.jphotobiol.2016.06.044.

[81] Montagni T, Enciso P, Marizcurrena JJ, Castro-Sowinski S, Fontana C, Davyt D. Dye sensitized solar cells based on Antarctic Hymenobacter sp. UV11 dyes. Environ Sustain 2018.

[82] Srivastava SK, Piwek P, Ayakar SR, Bonakdarpour A, Wilkinson DP, Yadav VG. A biogenic photovoltaic material. Small. https://doi.org/10.1002/smll.201800729; 2018.

[83] Mershin A, Matsumoto K, Kaiser L, Yu D, Vaughn M, Nazeeruddin MK, et al. Self-assembled photosystem-I biophotovoltaics on nanostructured TiO2 and ZnO. Sci Rep 2012. https://doi.org/10.1038/srep00234.

[84] Nazeeruddin MK, Baranoff E, Grätzel M. Dye-sensitized solar cells: a brief overview. Sol Energy 2011. https://doi.org/10.1016/j.solener.2011.01.018.

[85] Gong J, Sumathy K, Qiao Q, Zhou Z. Review on dye-sensitized solar cells (DSSCs): advanced techniques and research trends. Renew Sustain Energy Rev 2017. https://doi.org/10.1016/j.rser.2016.09.097.

[86] Kavan L. Electrochemistry of titanium dioxide: some aspects and highlights. Chem Rec 2012. https://doi.org/10.1002/tcr.201100012.

[87] Gong J, Liang J, Sumathy K. Review on dye-sensitized solar cells (DSSCs): fundamental concepts and novel materials. Renew Sustain Energy Rev 2012. https://doi.org/10.1016/j.rser.2012.04.044.

[88] Hagfeldt A, Grätzel M. Light-induced redox reactions in nanocrystalline systems. Chem Rev 1995. https://doi.org/10.1021/cr00033a003.

[89] Rühle S, Cahen D. Electron tunneling at the TiO2/substrate interface can determine dye-sensitized solar cell performance. J Phys Chem B 2004. https://doi.org/10.1021/jp047686s.

[90] Asbury JB, Hao E, Wang Y, Ghosh HN, Lian T. Ultrafast electron transfer dynamics from molecular adsorbates to semiconductor. J Phys Chem B 2001. https://doi.org/10.1021/jp003485m.

[91] Sarker S, Seo HW, Kim DM. Calculating current density-voltage curves of dye-sensitized solar cells: a straight-forward approach. J Power Sources 2014. https://doi.org/10.1016/j.jpowsour.2013.09.101.

[92] Halme J, Vahermaa P, Miettunen K, Lund P. Device physics of dye solar cells. Adv Mater 2010. https://doi.org/10.1002/adma.201000726.

[93] Jain A, Kapoor A. A new approach to study organic solar cell using Lambert W-function. Sol Energy Mater Sol Cells 2005. https://doi.org/10.1016/j.solmat.2004.07.004.

[94] Jain A, Kapoor A. A new method to determine the diode ideality factor of real solar cell using Lambert W-function. Sol Energy Mater Sol Cells 2005. https://doi.org/10.1016/j.solmat.2004.05.022.

[95] Yu H, Zhang S, Zhao H, Will G, Liu P. An efficient and low-cost TiO2 compact layer for performance improvement of dye-sensitized solar cells. Electrochim Acta 2009. https://doi.org/10.1016/j.electacta.2008.09.025.

[96] Cameron PJ, Peter LM, Hore S. How important is the back reaction of electrons via the substrate in dye-sensitized nanocrystalline solar cells? J Phys Chem B 2005. https://doi.org/10.1021/jp0405759.

[97] Cameron PJ, Peter LM. How does back-reaction at the conducting glass substrate influence the dynamic photovoltage response of nanocrystalline dye-sensitized solar cells? J Phys Chem B 2005. https://doi.org/10.1021/jp0407270.

[98] Glenn AR. Production of extracellular proteins by bacteria. Annu Rev Microbiol 1976;30:41–62.

[99] Ribosome. Nat Educ 2014. https://www.nature.com/scitable/definition/ribosome-194.

[100] Ribosomes Transcription, Translation. Nat Educ 2014. https://www.nature.com/scitable/topicpage/ribosomes-transcription-and-translation-14120660.

[101] Chandi GK, Gill BS. Production and characterization of microbial carotenoids as an alternative to synthetic colors: a review. Int J Food Prop 2011. https://doi.org/10.1080/10942910903256956.

[102] Barredo J-L. Microbial carotenoids from bacteria and microalgae. Methods and Protocols 2012. https://doi.org/10.1007/978-1-61779-879-5.

[103] Kirti K, Amita S, Priti S, Mukesh Kumar A, Jyoti S. Colorful world of microbes: carotenoids and their applications. Adv Biol 2014. https://doi.org/10.1155/2014/837891.

[104] Kay A, Graetzel M. Artificial photosynthesis. 1. Photosensitization of titania solar cells with chlorophyll derivatives and related natural porphyrins. J Phys Chem 1993. https://doi.org/10.1021/j100125a029.

[105] Ahmad S, Guillén E, Kavan L, Grätzel M, Nazeeruddin MK. Metal free sensitizer and catalyst for dye sensitized solar cells. Energy Environ Sci 2013. https://doi.org/10.1039/c3ee41888j.

[106] Cui Y, Wu Y, Lu X, Zhang X, Zhou G, Miapeh FB, et al. Incorporating benzotriazole moiety to construct D-A-π-A organic sensitizers for solar cells: significant enhancement of open-circuit photovoltage with long alkyl group. Chem Mater 2011. https://doi.org/10.1021/cm202226j.

[107] Nagai A, Takagi K. Conjugated objects: developments, synthesis, and applications. Pan Stanford; 2017.

[108] Lewis GN, Calvin M. The color of organic substances. Chem Rev 1939. https://doi.org/10.1021/cr60081a004.

[109] Samal A. Brief Discussion on Color: why does such conjugation allow absorption of visible light?. https://people.chem.umass.edu/samal/269/color.pdf; 2014.

[110] Caufield JH, Abreu M, Wimble C, Uetz P. Protein complexes in bacteria. PLoS Comput Biol 2015. https://doi.org/10.1371/journal.pcbi.1004107.

[111] Daviso E, Prakash S, Alia a, Gast P, Neugebauer J, Jeschke G, et al. The electronic structure of the primary electron donor of reaction centers of purple bacteria at atomic resolution as observed by photo-CIDNP 13C NMR. Proc Natl Acad Sci U S A 2009. https://doi.org/10.1073/pnas.0908608106.

[112] Bryant DA, Garcia Costas AM, Maresca JA, Chew AGM, Klatt CG, Bateson MM, et al. Candidates Chloracidobacterium thermophilum: an aerobic phototrophic acidobacterium. Science 2007. https://doi.org/10.1126/science.1143236.

[113] Fairhead M, Shen D, Chan LKM, Lowe ED, Donohoe TJ, Howarth M. Love-Hate ligands for high resolution analysis of strain in ultra-stable protein/small molecule interaction. Bioorg Med Chem 2014. https://doi.org/10.1016/j.bmc.2014.07.029.

[114] Gai F, Hasson KC, McDonald JC, Anfinrud PA. Chemical dynamics in proteins: the photoisomerization of retinal in bacteriorhodopsin. Science 1998. https://doi.org/10.1126/science.279.5358.1886. 80-.

[115] Yang Y, Yatsunami R, Ando A, Miyoko N, Fukui T, Takaichi S, et al. Complete biosynthetic pathway of the C50 carotenoid bacterioruberin from lycopene in the extremely halophilic archaeon Haloarcula japonica. J Bacteriol 2015. https://doi.org/10.1128/JB.02523-14.

[116] Dummer AM, Bonsall JC, Cihla JB, Lawry SM, Johnson GC, Peck RF. Bacterioopsin-Mediated regulation of bacterioruberin biosynthesis in Halobacterium salinarum. J Bacteriol 2011. https://doi.org/10.1128/JB.05376-11.

[117] Kim DJ, Takasuka N, Nishino H, Tsuda H. Chemoprevention of lung cancer by lycopene. Biofactors 2000. https://doi.org/10.1002/biof.5520130116.

[118] Magis GJ, den Hollander MJ, Onderwaater WG, Olsen JD, Hunter CN, Aartsma TJ, et al. Light harvesting, energy transfer and electron cycling of a native photosynthetic membrane adsorbed onto a gold surface. Biochim Biophys Acta Biomembr 2010. https://doi.org/10.1016/j.bbamem.2009.12.018.

[119] General introduction to the chemistry of dyes. IARC Monogr Eval Carcinog Risks to Humans; 2010.

[120] Sivakumar V, Wang R, Hastings G. Photo-oxidation of P740, the primary electron donor in photosystem I from acaryochloris marina. Biophys J 2003. https://doi.org/10.1016/S0006-3495(03)74734-1.

[121] Trammell SA, Wang L, Zullo JM, Shashidhar R, Lebedev N. Orientated binding of photosynthetic reaction centers on gold using Ni-NTA self-assembled monolayers. Biosens Bioelectron 2004. https://doi.org/10.1016/j.bios.2003.12.034.

[122] Zhao J, Zou Y, Liu B, Xu C, Kong J. Differentiating the orientations of photosynthetic reaction centers on Au electrodes linked by different bifunctional reagents. Biosens Bioelectron 2002. https://doi.org/10.1016/S0956-5663(02)00026-X.

[123] Feher G, Allen JP, Okamura MY, Rees DC. Structure and function of bacterial photosynthetic reaction centeres. Nature 1989. https://doi.org/10.1038/339111a0.

[124] Deisenhofer J, Michel H. The photosynthetic reaction center from the purple bacterium Rhodopseudomonas viridis. Science 1989. https://doi.org/10.1126/science.245.4925.1463. 80-.

[125] Franck H, Cogdell RJ. In: Young A, Britt G, editors. Photochemistry and function of carotenoids in photosynthesis. Carotenoids Photosynth.; 1993.

[126] Koyama Y, Fujii R. Cis-trans carotenoids in photosynthesis: configurations, excited-state properties and physiological functions. Photochem. carotenoids. Dordrecht: Springer; 1999. p. 161–88.

[127] Frank HA, Brudvig GW. Redox functions of carotenoids in photosynthesis. Biochemistry 2004. https://doi.org/10.1021/bi0492096.

[128] Groma GI, Szabó G, Váró G. Direct measurement of picosecond charge separation in bacteriorhodopsin. Nature 1984. https://doi.org/10.1038/308557a0.

[129] Váró G, Keszthelyi L. Photoelectric signals from dried oriented purple membranes of Halobacterium halobium. Biophys J 1983. https://doi.org/10.1016/S0006-3495(83)84322-7.

[130] Dworkin M, Falkow S. The prokaryotes: archaea. Bacteria: firmicutes, actinomycetes; 2006.

[131] Ito S, Murakami TN, Comte P, Liska P, Grätzel C, Nazeeruddin MK, et al. Fabrication of thin film dye sensitized solar cells with solar to electric power conversion efficiency over 10%. Thin Solid Films 2008. https://doi.org/10.1016/j.tsf.2007.05.090.

[132] Minton KW. DNA repair in the extremely radioresistant bacterium Deinococcus radiodurans. Mol Microbiol 1994. https://doi.org/10.1111/j.1365-2958.1994.tb00937.x.

[133] Fernández Zenoff V, Siñeriz F, Farías ME. Diverse responses to UV-B radiation and repair mechanisms of bacteria isolated from high-altitude aquatic environments. Appl Environ Microbiol 2006. https://doi.org/10.1128/AEM.01333-06.

[134] Correa-Llantén DN b, Amenábar MJ, Blamey JM. Antioxidant capacity of novel pigments from an Antarctic bacterium. J Microbiol 2012. https://doi.org/10.1007/s12275-012-2029-1.

[135] Fujii M, Takano Y, Kojima H, Hoshino T, Tanaka R, Fukui M. Microbial community structure, pigment composition, and nitrogen source of red snow in Antarctica. Microb Ecol 2010. https://doi.org/10.1007/s00248-009-9594-9.

[136] Zhuang T, Sasaki SI, Ikeuchi T, Kido J, Wang XF. Natural-photosynthesis-inspired photovoltaic cells using carotenoid aggregates as electron donors and chlorophyll derivatives as electron acceptors. RSC Adv 2015. https://doi.org/10.1039/c5ra07099f.

[137] Freitag M, Teuscher J, Saygili Y, Zhang X, Giordano F, Liska P, et al. Dye-sensitized solar cells for efficient power generation under ambient lighting. Nat Photonics 2017. https://doi.org/10.1038/nphoton.2017.60.

[138] Zhou H, Wu L, Gao Y, Ma T. Dye-sensitized solar cells using 20 natural dyes as sensitizers. J Photochem Photobiol A Chem 2011. https://doi.org/10.1016/j.jphotochem.2011.02.008.

[139] Calogero G, Yum JH, Sinopoli A, Di Marco G, Grätzel M, Nazeeruddin MK. Anthocyanins and betalains as light-harvesting pigments for dye-sensitized solar cells. Sol Energy 2012. https://doi.org/10.1016/j.solener.2012.02.018.

[140] Hao S, Wu J, Huang Y, Lin J. Natural dyes as photosensitizers for dye-sensitized solar cell. Sol Energy 2006. https://doi.org/10.1016/j.solener.2005.05.009.

[141] Mori S, Nagata M, Nakahata Y, Yasuta K, Goto R, Kimura M, et al. Enhancement of incident photon-to-current conversion efficiency for phthalocyanine-sensitized solar cells by 3D molecular structuralization. J Am Chem Soc 2010. https://doi.org/10.1021/ja9109677.

[142] Ikeuchi T, Nomoto H, Masaki N, Griffith MJ, Mori S, Kimura M. Molecular engineering of zinc phthalocyanine sensitizers for efficient dye-sensitized solar cells. Chem Commun 2014. https://doi.org/10.1039/c3cc47714b.

[143] Wu W, Hua J, Jin Y, Zhan W, Tian H. Photovoltaic properties of three new cyanine dyes for dye-sensitized solar cells. Photochem Photobiol Sci 2007. https://doi.org/10.1039/b712439b.

[144] Ma X, Hua J, Wu W, Jin Y, Meng F, Zhan W, et al. A high-efficiency cyanine dye for dye-sensitized solar cells. Tetrahedron 2008. https://doi.org/10.1016/j.tet.2007.10.094.

[145] Karki IB, Nakarmi JJ, Mandal PK, Chatterjee S. Effect of organic dyes on the performance of ZnO based dye-sensitized solar cells. Appl Sol Energy 2013. https://doi.org/10.3103/s0003701x13010052.

[146] Hara K, Kurashige M, Dan-Oh Y, Kasada C, Shinpo A, Suga S, et al. Design of new coumarin dyes having thiophene moieties for highly efficient organic-dye-sensitized solar cells. New J Chem 2003. https://doi.org/10.1039/b300694h.

[147] Wang ZS, Cui Y, Hara K, Dan-Oh Y, Kasada C, Shinpo A. A high-light-harvesting-efficiency coumarin dye for stable dye-sensitized solar cells. Adv Mater 2007. https://doi.org/10.1002/adma.200601020.

[148] Zanjanchi F, Beheshtian J. Natural pigments in dye-sensitized solar cell (DSSC): a DFT-TDDFT study. J Iran Chem Soc 2019. https://doi.org/10.1007/s13738-018-1561-2.

[149] Pandey AK, Ahmad MS, Rahim NA, Tyagi VV, Saidur R. Natural sensitizers and their applications in dye-sensitized solar cell. Environ. Biotechnol. Sustain. Futur. 2018. https://doi.org/10.1007/978-981-10-7284-0_15.

[150] Kumara GRA, Kaneko S, Okuya M, Onwona-Agyeman B, Konno A, Tennakone K. Shiso leaf pigments for dye-sensitized solid-state solar cell. Sol Energy Mater Sol Cells 2006. https://doi.org/10.1016/j.solmat.2005.07.007.

[151] Ghann W, Kang H, Sheikh T, Yadav S, Chavez-Gil T, Nesbitt F, et al. Fabrication, optimization and characterization of natural dye sensitized solar cell. Sci Rep 2017. https://doi.org/10.1038/srep41470.

[152] Sanjay P, Deepa K, Madhavan J, Senthil S. Performance of TiO2 based dye-sensitized solar cells fabricated with dye extracted from leaves of Peltophorum pterocarpum and Acalypha amentacea as sensitizer. Mater Lett 2018. https://doi.org/10.1016/j.matlet.2018.02.085.

[153] Iqbal MZ, Ali SR, Khan S. Progress in dye sensitized solar cell by incorporating natural photosensitizers. Sol Energy 2019. https://doi.org/10.1016/j.solener.2019.02.023.

[154] Gómez-Ortíz NM, Vázquez-Maldonado IA, Pérez-Espadas AR, Mena-Rejón GJ, Azamar-Barrios JA, Oskam G. Dye-sensitized solar cells with natural dyes extracted from achiote seeds. Sol Energy Mater Sol Cells 2010. https://doi.org/10.1016/j.solmat.2009.05.013.

[155] Wang XF, Zhan CH, Maoka T, Wada Y, Koyama Y. Fabrication of dye-sensitized solar cells using chlorophylls c1 and c2 and their oxidized forms c1′ and c2′ from Undaria pinnatifida (Wakame). Chem Phys Lett 2007. https://doi.org/10.1016/j.cplett.2007.08.097.

[156] Calogero G, Bartolotta A, Di Marco G, Di Carlo A, Bonaccorso F. Vegetable-based dye-sensitized solar cells. Chem Soc Rev 2015. https://doi.org/10.1039/c4cs00309h.

[157] Cao Y, Saygili Y, Ummadisingu A, Teuscher J, Luo J, Pellet N, et al. 11% efficiency solid-state dye-sensitized solar cells with copper(II/I) hole transport materials. Nat Commun 2017. https://doi.org/10.1038/ncomms15390.

[158] Godibo DJ, Anshebo ST, Anshebo TY. Dye sensitized solar cells using natural pigments from five plants and Quasi-solid state electrolyte. J Braz Chem Soc 2015. https://doi.org/10.5935/0103-5053.20140218.

[159] Bella F, Pugliese D, Zolin L, Gerbaldi C. Paper-based quasi-solid dye-sensitized solar cells. Electrochim Acta 2017. https://doi.org/10.1016/j.electacta.2017.03.211.

[160] Rapsomanikis A, Sygkridou D, Voutsinas E, Stathatos E. Transparent quasi-solid state dye-sensitized solar cells sensitized with naturally derived pigment extracted from red seaweed. Curr Appl Phys 2016. https://doi.org/10.1016/j.cap.2016.03.018.

[161] Suzuka M, Hayashi N, Sekiguchi T, Sumioka K, Takata M, Hayo N, et al. A quasi-solid state DSSC with 10.1% efficiency through molecular design of the charge-separation and -transport. Sci Rep 2016. https://doi.org/10.1038/srep28022.

[162] Yazie N, Worku D, Reda A. Natural dye as Light-Harvesting pigments for Quasi-Solid-State Dye-Sensitized solar cells. Mater Renew Sustain Energy 2016. https://doi.org/10.1007/s40243-016-0077-x.

[163] Kumar Y, Florvall L. Convenient synthesis of indolines by reduction of indoles with sodium cyanoborohydride in carboxylic acids. Synth Commun 1983. https://doi.org/10.1080/00397918308081827.

[164] Britannica. Indole (benzopyrrole). Encycl Br 2018. https://www.britannica.com/science/indole.

[165] Bhandari S, Mondal D, Nataraj SK, Balakrishna RG. Biomolecule-derived quantum dots for sustainable optoelectronics. Nanoscale Adv 2019. https://doi.org/10.1039/c8na00332g.

[166] Mansour R. Natural dyes and pigments: extraction and applications. Handb. Renew. Mater. Color. Finish. 2018.

[167] Furuichi K, Sashima T, Koyama Y. The first detection of the 3Ag- state in carotenoids using resonance-Raman excitation profiles. Chem Phys Lett 2002. https://doi.org/10.1016/S0009-2614(02)00412-8.

[168] Shahmohammadi HR, Asgarani E, Terato H, Saito T, Ohyama Y, Gekko K, et al. Protective roles of bacterioruberin and intracellular KCl in the resistance of Halobacterium salinarium against DNA-damaging agents. J Radiat Res 1998. https://doi.org/10.1269/jrr.39.251.

[169] Gallardo C, Monrás JP, Plaza DO, Collao B, Saona LA, Durán-Toro V, et al. Low-temperature biosynthesis of fluorescent semiconductor nanoparticles (CdS) by oxidative stress resistant Antarctic bacteria. J Biotechnol 2014. https://doi.org/10.1016/j.jbiotec.2014.07.017.

[170] Plaza DO, Gallardo C, Straub YD, Bravo D, Pérez-Donoso JM. Biological synthesis of fluorescent nanoparticles by cadmium and tellurite resistant Antarctic bacteria: exploring novel natural nanofactories. Microb Cell Factories 2016. https://doi.org/10.1186/s12934-016-0477-8.

[171] Iwuchukwu IJ, Vaughn M, Myers N, O'Neill H, Frymier P, Bruce BD. Self-organized photosynthetic nanoparticle for cell-free hydrogen production. Nat Nanotechnol 2010. https://doi.org/10.1038/nnano.2009.315.

[172] Ferreira GB, Hollauer E, Comerlato NM, Wardell JL. An experimental and theoretical study of the electronic spectra of tetraethylammonium [bis(1,3-dithiole-2-thione-4,5-dithiolato)M(III)] and tetraethylammonium [bis(1,3-dithiole-2-one-4,5-dithiolato)M(III)] (M = Sb or Bi). Spectrochim Acta Part A Mol Biomol Spectrosc 2008. https://doi.org/10.1016/j.saa.2007.12.010.

[173] Ramachandran CN, Roy D, Sathyamurthy N. Host-guest interaction in endohedral fullerenes. Chem Phys Lett 2008. https://doi.org/10.1016/j.cplett.2008.06.073.

[174] Losito I, Palmisano F, Zambonin PG. o-phenylenediamine electropolymerization by cyclic voltammetry combined with electrospray ionization-ion trap mass spectrometry. Anal Chem 2003. https://doi.org/10.1021/ac0342424.

[175] Janietz S, Bradley DDC, Grell M, Giebeler C, Inbasekaran M, Woo EP. Electrochemical determination of the ionization potential and electron affinity of poly(9,9-dioctylfluorene). Appl Phys Lett 1998. https://doi.org/10.1063/1.122479.

[176] Kim Y-S, Shin J-I, Park S-Y, Jun K, Son Y-A. Electrochemical studies on heptamethine cyanine dyes. Text Color Finish 2013. https://doi.org/10.5764/tcf.2009.21.5.035.

[177] Calogero G, Sinopoli A, Citro I, Di Marco G, Petrov V, Diniz AM, et al. Synthetic analogues of anthocyanins as sensitizers for dye-sensitized solar cells. Photochem Photobiol Sci 2013. https://doi.org/10.1039/c3pp25347c.

[178] Ruiz-Anchondo T, Flores-Holguín N, Glossman-Mitnik D. Natural carotenoids as nanomaterial precursors for molecular photovoltaics: a computational DFT study. Molecules 2010. https://doi.org/10.3390/molecules15074490.

[179] Martins JBL, Durães JA, Sales MJA, Vilela ASFA, Silva GME, Gargano R. Theoretical investigation of carotenoid ultraviolet spectra. Int J Quantum Chem 2009. https://doi.org/10.1002/qua.21845.

[180] Wang XF, Tamiaki H, Kitao O, Ikeuchi T, Sasaki SI. Molecular engineering on a chlorophyll derivative, chlorin e6, for significantly improved power conversion efficiency in dye-sensitized solar cells. J Power Sources 2013. https://doi.org/10.1016/j.jpowsour.2013.05.191.

[181] Castro FA, Faes A, Geiger T, Graeff CFO, Nagel M, Nüesch F, et al. On the use of cyanine dyes as low-bandgap materials in bulk heterojunction photovoltaic devices. Synth Met 2006. https://doi.org/10.1016/j.synthmet.2006.06.010.

[182] Liu K, Yao Y, Wang J, Zhu L, Sun M, Ren B, et al. Spiro[fluorene-9,9′-xanthene]-based hole transporting materials for efficient perovskite solar cells with enhanced stability. Mater Chem Front 2017. https://doi.org/10.1039/c6qm00097e.

[183] Qian Y, Ni Y, Yue S, Li W, Chen S, Zhang Z, et al. Spiro[fluorene-9,9′-xanthene]-based universal hosts for understanding structure-property relationships in RGB and white PhOLEDs. RSC Adv 2015. https://doi.org/10.1039/c5ra00694e.

[184] Carbas BB, Önal AM. New fluorene-xanthene-based hybrid electrochromic and fluorescent polymers via donor-acceptor approach. Electrochim Acta 2012. https://doi.org/10.1016/j.electacta.2012.01.026.

[185] Sánchez-De-Armas R, San Miguel MÁ, Oviedo J, Sanz JF. Coumarin derivatives for dye sensitized solar cells: a TD-DFT study. Phys Chem Chem Phys 2012. https://doi.org/10.1039/c1cp22058f.

[186] Agrawal S, Dev P, English NJ, Thampi KR, MacElroy JMD. First-principles study of the excited-state properties of coumarin-derived dyes in dye-sensitized solar cells. J Mater Chem 2011;21:11101–8.

[187] Willinger K, Thelakkat M. Photosensitizers in solar energy conversion. Photosensit. Med. Environ. Secur. 2014. https://doi.org/10.1007/978-90-481-3872-2_11.

[188] Burschka J, Pellet N, Moon SJ, Humphry-Baker R, Gao P, Nazeeruddin MK, et al. Sequential deposition as a route to high-performance perovskite-sensitized solar cells. Nature 2013. https://doi.org/10.1038/nature12340.

[189] McGehee MD. Materials science: fast-track solar cells. Nature 2013;501:323.

[190] Mehmood U, Rahman SU, Harrabi K, Hussein IA, Reddy BVS. Recent advances in dye sensitized solar cells. Ann Mater Sci Eng 2014. https://doi.org/10.1155/2014/974782.

[191] Grätzel M. Recent advances in sensitized mesoscopic solar cells. Acc Chem Res 2009. https://doi.org/10.1021/ar900141y.

[192] Mehmood U, Al-Ahmed A, Al-Sulaiman FA, Malik MI, Shehzad F, Khan AUH. Effect of temperature on the photovoltaic performance and stability of solid-state dye-sensitized solar cells: a review. Renew Sustain Energy Rev 2017. https://doi.org/10.1016/j.rser.2017.05.114.

[193] Yang H, Huang M, Wu J, Lan Z, Hao S, Lin J. The polymer gel electrolyte based on poly(methyl methacrylate) and its application in quasi-solid-state dye-sensitized solar cells. Mater Chem Phys 2008. https://doi.org/10.1016/j.matchemphys.2008.01.010.

[194] Kim JH, Moon KJ, Kim JM, Lee D, Kim SH. Effects of various light-intensity and temperature environments on the photovoltaic performance of dye-sensitized solar cells. Sol Energy 2015. https://doi.org/10.1016/j.solener.2015.01.012.

[195] Bari D, Wrachien N, Tagliaferro R, Penna S, Brown TM, Reale A, et al. Thermal stress effects on dye-sensitized solar cells (DSSCs). Microelectron Reliab 2011. https://doi.org/10.1016/j.microrel.2011.07.061.

[196] Berginc M, Opara Krašovec U, Hočevar M, Topič M. Performance of dye-sensitized solar cells based on Ionic liquids: effect of temperature and iodine concentration. Thin Solid Films 2008. https://doi.org/10.1016/j.tsf.2007.12.003.

[197] Lobato K, Peter LM. Direct measurement of the temperature coefficient of the electron quasi-Fermi level in dye-sensitized nanocrystalline solar cells using a titanium sensor electrode. J Phys Chem B 2006. https://doi.org/10.1021/jp064538o.

[198] Snaith HJ, Schmidt-Mende L, Grätzel M, Chiesa M. Light intensity, temperature, and thickness dependence of the open-circuit voltage in solid-state dye-sensitized solar cells. Phys Rev B Condens Matter Mater Phys 2006. https://doi.org/10.1103/PhysRevB.74.045306.

[199] Wang M, Chen P, Humphry-Baker R, Zakeeruddin SM, Grätzel M. The influence of charge transport and recombination on the performance of dye-sensitized solar cells. ChemPhysChem 2009. https://doi.org/10.1002/cphc.200800708.

[200] Maçaira J, Mesquita I, Andrade L, Mendes A. Role of temperature in the recombination reaction on dye-sensitized solar cells. Phys Chem Chem Phys 2015. https://doi.org/10.1039/c5cp02942b.

[201] Cameron PJ, Peter LM. Characterization of titanium dioxide blocking layers in dye-sensitized nanocrystalline solar cells. J Phys Chem B 2003. https://doi.org/10.1021/jp030790+.

[202] Zhiqun Lin JW. Low-cost nanomaterials: toward greener and more efficient energy applications. Springer; 2014.

[203] Thomas Sabu, Mamour Sakho El Hadji, Kalarikkal Nandakumar, Oluwafemi Oluwatobi Samuel. Nanomaterials for solar cell applications. Elsevier; 2019.

[204] Gavin Conibeer, Nozik Arthur J, Matthew C, Beard Nozik AJ, Conibeer G, Beard MC. Advanced concepts in photovoltaics. Royal Society of Chemistry 2014.

[205] Gu F, Huang W, Wang S, Cheng X, Hu Y, Lee PS. Open-circuit voltage improvement in tantalum-doped TiO$_2$ nanocrystals. Phys Chem Chem Phys 2014. https://doi.org/10.1039/c4cp01655f.

[206] Berginc M, Opara Krašovec U, Jankovec M, Topič M. The effect of temperature on the performance of dye-sensitized solar cells based on a propyl-methyl-imidazolium iodide electrolyte. Sol Energy Mater Sol Cells 2007. https://doi.org/10.1016/j.solmat.2007.02.001.

[207] Grätzel M. Photovoltaic performance and long-term stability of dye-sensitized meososcopic solar cells. Compt Rendus Chem 2006. https://doi.org/10.1016/j.crci.2005.06.037.

[208] Wang R, Xue J, Meng L, Lee J-W, Zhao Z, Sun P, et al. Caffeine improves the performance and thermal stability of perovskite solar cells. Joule 2019. https://doi.org/10.1016/j.joule.2019.04.005.

[209] Steirer KX, Reese MO, Rupert BL, Kopidakis N, Olson DC, Collins RT, et al. Ultrasonic spray deposition for production of organic solar cells. Sol Energy Mater Sol Cells 2009. https://doi.org/10.1016/j.solmat.2008.10.026.

[210] Layani M, Gruchko M, Milo O, Balberg I, Azulay D, Magdassi S. Transparent conductive coatings by printing coffee ring arrays obtained at room temperature. ACS Nano 2009. https://doi.org/10.1021/nn901239z.

[211] Singh BR, Wechter MA, Hu Y, Lafontaine C. Determination of caffeine content in coffee using fourier transform infra-red spectroscopy in combination with attenuated total reflectance technique: a bioanalytical chemistry experiment for biochemists. Biochem Educ 1998. https://doi.org/10.1016/S0307-4412(98)00078-8.

[212] Hou X, Huang S, Ou-Yang W, Pan L, Sun Z, Chen X. Constructing efficient and stable perovskite solar cells via interconnecting perovskite grains. ACS Appl Mater Interfaces 2017. https://doi.org/10.1021/acsami.7b08488.

[213] Kang HY, Wang HP. Cu@C dispersed TiO2for dye-sensitized solar cell photoanodes. Appl Energy 2012. https://doi.org/10.1016/j.apenergy.2012.03.004.

[214] Luque de Castro MD, Priego-Capote F. Soxhlet extraction: past and present panacea. J Chromatogr A 2010. https://doi.org/10.1016/j.chroma.2009.11.027.

[215] Click KA, Schockman BM, Dilenschneider JT, McCulloch WD, Garrett BR, Yu Y, et al. Bilayer dye protected aqueous photocathodes for tandem dye-sensitized solar cells. J Phys Chem C 2017. https://doi.org/10.1021/acs.jpcc.7b01911.

[216] Lee K, Park SW, Ko MJ, Kim K, Park NG. Selective positioning of organic dyes in a mesoporous inorganic oxide film. Nat Mater 2009. https://doi.org/10.1038/nmat2475.

[217] Fredin K, Rühle S, Grasso C, Hagfeldt A. Studies of coupled charge transport in dye-sensitized solar cells using a numerical simulation tool. Sol Energy Mater Sol Cells 2006. https://doi.org/10.1016/j.solmat.2005.12.004.

[218] Kuciauskas D, Freund MS, Gray HB, Winkler JR, Lewis NS. Electron transfer dynamics in nanocrystalline titanium dioxide solar cells sensitized with ruthenium or osmium polypyridyl complexes. J Phys Chem B 2001. https://doi.org/10.1021/jp002545l.

[219] Clifford JN, Palomares E, Nazeeruddin MK, Grätzel M, Nelson J, Li X, et al. Molecular control of recombination dynamics in dye-sensitized nanocrystalline TiO2 films: free energy vs distance dependence. J Am Chem Soc 2004. https://doi.org/10.1021/ja039924n.

[220] Haque SA, Handa S, Peter K, Palomares E, Thelakkat M, Durrant JR. Supermolecular control of charge transfer in dye-sensitized nanocrystalline TiO$_2$ films: towards a quantitative structure-function relationship. Angew Chem Int Ed 2005. https://doi.org/10.1002/anie.200500363.

[221] Clifford JN, Yahioglu G, Milgrom LR, Durrant JR. Molecular control of recombination dynamics in dye sensitised nanocrystalline TiO$_2$ films. Chem Commun 2002. https://doi.org/10.1039/b201855a.

[222] Wiberg J, Marinado T, Hagberg DP, Sun L, Hagfeldt A, Albinsson B. Effect of anchoring group on electron injection and recombination dynamics in organic dye-sensitized solar cells. J Phys Chem C 2009. https://doi.org/10.1021/jp8101139.

[223] Nazeeruddin MK, Kay A, Rodicio I, Humphry-Baker R, Müller E, Liska P, et al. Conversion of light to electricity by cis-X$_2$Bis (2,2′-bipyridyl-4,4′-dicarboxylate) ruthenium (II) charge-transfer sensitizers (X = Cl−, Br−, I−, CN−, and SCN−) on nanocrystalline TiO$_2$ Electrodes. J Am Chem Soc 1993. https://doi.org/10.1021/ja00067a063.

[224] Miyashita M, Sunahara K, Nishikawa T, Uemura Y, Koumura N, Hara K, et al. Interfacial electron-transfer kinetics in metal-free organic dye-sensitized solar cells: combined effects of molecular structure of dyes and electrolytes. J Am Chem Soc 2008. https://doi.org/10.1021/ja803534u.

[225] Koumura N, Wang ZS, Mori S, Miyashita M, Suzuki E, Hara K. Alkyl-functionalized organic dyes for efficient molecular photovoltaics. J Am Chem Soc 2006. https://doi.org/10.1021/ja0645640.

[226] O'Regan BC, López-Duarte I, Martínez-Díaz MV, Forneli A, Albero J, Morandeira A, et al. Catalysis of recombination and its limitation on open circuit voltage for dye sensitized photovoltaic cells using phthalocyanine dyes. J Am Chem Soc 2008. https://doi.org/10.1021/ja078045o.

[227] O'Regan BC, Walley K, Juozapavicius M, Anderson A, Matar F, Ghaddar T, et al. Structure/function relationships in dyes for solar energy conversion: a two-atom change in dye structure and the mechanism for its effect on cell voltage. J Am Chem Soc 2009. https://doi.org/10.1021/ja806869x.

[228] Reynal A, Forneli A, Martinez-Ferrero E, Sánchez-Díaz A, Vidal-Ferran A, O'Regan BC, et al. Interfacial charge recombination between e⁻-TiO$_2$ and the I⁻/I$_3$ electrolyte in ruthenium heteroleptic complexes: dye molecular structure-open circuit voltage relationship. J Am Chem Soc 2008. https://doi.org/10.1021/ja800513m.

[229] Palomares E, Clifford JN, Haque SA, Lutz T, Durrant JR. Control of charge recombination dynamics in dye sensitized solar cells by the use of conformally deposited metal oxide blocking layers. J Am Chem Soc 2003. https://doi.org/10.1021/ja027945w.

[230] Wang H, Hu YH. Graphene as a counter electrode material for dye-sensitized solar cells. Energy Environ Sci 2012;5:8182–8.

[231] Gomesh N, Ibrahim AH, Syafinar R, Irwanto M, Mamat MR, M Irwan Y, Hashim2 NM U. Fabrication of dye sensitized solar cell using various counter electrode thickness. Int J Ser Eng Sci 2015;1:49–65.

[232] Sahito IA, Sun KC, Arbab AA, Qadir MB, Choi YS, Jeong SH. Flexible and conductive cotton fabric counter electrode coated with graphene nanosheets for high efficiency dye sensitized solar cell. J Power Sources 2016. https://doi.org/10.1016/j.jpowsour.2016.04.025.

[233] Wang H, Sun K, Tao F, Stacchiola DJ, Hu YH. 3D honeycomb-like structured graphene and its high efficiency as a counter-electrode catalyst for dye-sensitized solar cells. Angew Chem Int Ed 2013. https://doi.org/10.1002/anie.201303497.

[234] Yen YS, Chou HH, Chen YC, Hsu CY, Lin JT. Recent developments in molecule-based organic materials for dye-sensitized solar cells. J Mater Chem 2012. https://doi.org/10.1039/c2jm30362k.

[235] Papageorgiou N, Maier WF, Grätzel M. An iodine/triiodide reduction electrocatalyst for aqueous and organic media. J Electrochem Soc 1997. https://doi.org/10.1149/1.1837502.

[236] Papageorgiou N. An iodine/triiodide reduction electrocatalyst for aqueous and organic media. J Electrochem Soc 2006. https://doi.org/10.1149/1.1837502.

[237] Kim SS, Na SI, Jo J, Kim DY, Nah YC. Plasmon enhanced performance of organic solar cells using electrodeposited Ag nanoparticles. Appl Phys Lett 2008. https://doi.org/10.1063/1.2967471.

[238] Fang X, Ma T, Guan G, Akiyama M, Kida T, Abe E. Effect of the thickness of the Pt film coated on a counter electrode on the performance of a dye-sensitized solar cell. J Electroanal Chem 2004. https://doi.org/10.1016/j.jelechem.2004.04.004.

[239] Kay A, Grätzel M. Low cost photovoltaic modules based on dye sensitized nanocrystalline titanium dioxide and carbon powder. Sol Energy Mater Sol Cells 1996. https://doi.org/10.1016/0927-0248(96)00063-3.

[240] Imoto K, Takahashi K, Yamaguchi T, Komura T, Nakamura JI, Murata K. High-performance carbon counter electrode for dye-sensitized solar cells. Sol Energy Mater Sol Cells 2003. https://doi.org/10.1016/S0927-0248(03)00021-7.

[241] Suzuki K, Yamaguchi M, Kumagai M, Yanagida S. Application of carbon nanotubes to counter electrodes of dye-sensitized solar cells. Chem Lett 2002. https://doi.org/10.1246/cl.2003.28.

[242] Lee WJ, Ramasamy E, Lee DY, Song JS. Efficient dye-sensitized solar cells with catalytic multiwall carbon nanotube counter electrodes. ACS Appl Mater Interfaces 2009. https://doi.org/10.1021/am800249k.

[243] Li Z, Gong F, Zhou G, Wang ZS. NiS2/reduced graphene oxide nanocomposites for efficient dye-sensitized solar cells. J Phys Chem C 2013. https://doi.org/10.1021/jp401032c.

[244] Xue Y, Liu J, Chen H, Wang R, Li D, Qu J, et al. Nitrogen-doped graphene foams as metal-free counter electrodes in high-performance dye-sensitized solar cells. Angew Chem Int Ed 2012. https://doi.org/10.1002/anie.201207277.

[245] Meng X, Yu C, Song X, Liu Y, Liang S, Liu Z, et al. Nitrogen-doped graphene nanoribbons with surface enriched active sites and enhanced performance for dye-sensitized solar cells. Adv Energy Mater 2015. https://doi.org/10.1002/aenm.201500180.

[246] Ju MJ, Kim JC, Choi HJ, Choi IT, Kim SG, Lim K, et al. N-doped graphene nanoplatelets as superior metal-free counter electrodes for organic dye-sensitized solar cells. ACS Nano 2013. https://doi.org/10.1021/nn4009774.

[247] Luo Q, Hao F, Wang S, Shen H, Zhao L, Li J, et al. Highly efficient metal-free sulfur-doped and nitrogen and sulfur dual-doped reduced graphene oxide counter electrodes for dye-sensitized solar cells. J Phys Chem C 2014. https://doi.org/10.1021/jp5004424.

[248] Xue Y, Baek JM, Chen H, Qu J, Dai L. N-doped graphene nanoribbons as efficient metal-free counter electrodes for disulfide/thiolate redox mediated DSSCs. Nanoscale 2015. https://doi.org/10.1039/c4nr06969b.

[249] Mao S, Lu G, Chen J. Three-dimensional graphene-based composites for energy applications. Nanoscale 2015. https://doi.org/10.1039/c4nr06609j.

[250] Tang B, Hu G, Gao H, Shi Z. Three-dimensional graphene network assisted high performance dye sensitized solar cells. J Power Sources 2013. https://doi.org/10.1016/j.jpowsour.2013.01.130.

[251] Kim JY, Lee JY, Shin KY, Jeong H, Son HJ, Lee CH, et al. Highly crumpled graphene nano-networks as electrocatalytic counter electrode in photovoltaics. Appl Catal B Environ 2016. https://doi.org/10.1016/j.apcatb.2016.04.008.

[252] Sahito IA, Sun KC, Arbab AA, Qadir MB, Jeong SH. Graphene coated cotton fabric as textile structured counter electrode for DSSC. Electrochim Acta 2015. https://doi.org/10.1016/j.electacta.2015.05.035.

[253] Ye M, Wen X, Wang M, Iocozzia J, Zhang N, Lin C, et al. Recent advances in dye-sensitized solar cells: from photoanodes, sensitizers and electrolytes to counter electrodes. Mater Today 2015. https://doi.org/10.1016/j.mattod.2014.09.001.

[254] Faber MS, Park K, Cabán-Acevedo M, Santra PK, Jin S. Earth-abundant cobalt pyrite (CoS₂) thin film on glass as a robust, high-performance counter electrode for quantum dot-sensitized solar cells. J Phys Chem Lett 2013. https://doi.org/10.1021/jz400642e.

[255] Chang SH, Lu M De, Tung YL, Tuan HY. Gram-scale synthesis of catalytic Co9S8 nanocrystal ink as a cathode material for spray-deposited, large-area dye-sensitized solar cells. ACS Nano 2013. https://doi.org/10.1021/nn404272j.

[256] Yao RY, Zhou ZJ, Hou ZL, Wang X, Zhou WH, Wu SX. Surfactant-free CuInS₂ nanocrystals: an alternative counter-electrode material for dye-sensitized solar cells. ACS Appl Mater Interfaces 2013. https://doi.org/10.1021/am400031w.

[257] Yuan SJ, Zhou ZJ, Hou ZL, Zhou WH, Yao RY, Zhao Y, et al. Enhanced performance of dye-sensitized solar cells using solution-based in situ synthesis and fabrication of Cu₂ZnSnSe₄ nanocrystal counter electrode. Chem Eur J 2013. https://doi.org/10.1002/chem.201300283.

[258] Zhang H, Ge M, Yang L, Zhou Z, Chen W, Li Q, et al. Synthesis and catalytic properties of Sb₂S₃ nanowire bundles as counter electrodes for dye-sensitized solar cells. J Phys Chem C 2013. https://doi.org/10.1021/jp4016917.

[259] Mali SS, Patil PS, Hong CK. Low-cost electrospun highly crystalline kesterite Cu₂ZnSnS₄ nanofiber counter electrodes for efficient dye-sensitized solar cells. ACS Appl Mater Interfaces 2014. https://doi.org/10.1021/am404586n.

[260] Zhao Y, Ma X, Wang Z, Xu T, Wu W, Fong H. Electrospun TiC/C composite nanofibrous felt and its energy-related applications. Electrospun Nanofibers 2016. https://doi.org/10.1016/B978-0-08-100907-9.00014-3.

[261] Wei W, Wang H, Hu YH. Unusual particle-size-induced promoter-to-poison transition of ZrN in counter electrodes for dye-sensitized solar cells. J Mater Chem A 2013. https://doi.org/10.1039/c3ta13002a.

[262] Wen Z, Cui S, Pu H, Mao S, Yu K, Feng X, et al. Metal nitride/graphene nanohybrids: general synthesis and multifunctional titanium nitride/graphene electrocatalyst. Adv Mater 2011. https://doi.org/10.1002/adma.201102772.

[263] Wu MS, Wu JF. Pulse-reverse electrodeposition of transparent nickel phosphide film with porous nanospheres as a cost-effective counter electrode for dye-sensitized solar cells. Chem Commun 2013. https://doi.org/10.1039/c3cc45670f.

[264] Guo J, Shi Y, Chu Y, Ma T. Highly efficient telluride electrocatalysts for use as Pt-free counter electrodes in dye-sensitized solar cells. Chem Commun 2013. https://doi.org/10.1039/c3cc45698f.

[265] Trevisan R, Döbbelin M, Boix PP, Barea EM, Tena-Zaera R, Mora-Seró I, et al. PEDOT nanotube Arrays as high performing counter electrodes for dye sensitized solar cells. Study of the interactions among electrolytes and counter electrodes. Adv Energy Mater 2011. https://doi.org/10.1002/aenm.201100324.

[266] Xia J, Chen L, Yanagida S. Application of polypyrrole as a counter electrode for a dye-sensitized solar cell. J Mater Chem 2011. https://doi.org/10.1039/c0jm04116e.

[267] Bu C, Tai Q, Liu Y, Guo S, Zhao X. A transparent and stable polypyrrole counter electrode for dye-sensitized solar cell. J Power Sources 2013. https://doi.org/10.1016/j.jpowsour.2012.07.117.

[268] Sun W, Peng T, Liu Y, Xu S, Yuan J, Guo S, et al. Hierarchically porous hybrids of polyaniline nanoparticles anchored on reduced graphene oxide sheets as counter electrodes for dye-sensitized solar cells. J Mater Chem A 2013. https://doi.org/10.1039/c2ta01000c.

[269] Chen J, Li B, Zheng J, Zhao J, Jing H, Zhu Z. Polyaniline nanofiber/carbon film as flexible counter electrodes in platinum-free dye-sensitized solar cells. Electrochim Acta 2011. https://doi.org/10.1016/j.electacta.2011.02.097.

[270] Cho S, Hwang SH, Kim C, Jang J. Polyaniline porous counter-electrodes for high performance dye-sensitized solar cells. J Mater Chem 2012. https://doi.org/10.1039/c2jm30594a.